POLITECNICO
MILANO 1863

SCUOLA DI INGEGNERIA INDUSTRIALE
E DELL'INFORMAZIONE

Change Detection in Water Surface Area of Urmia Lake Using Landsat Imagery and Geographic Information System

TESI DI LAUREA MAGISTRALE IN
ENVIRONMENTAL AND LAND PLANNING ENGINEERING
INGEGNERIA PER L'AMBIENTE E IL TERRITORIO

Author: **SAHAR JAZAYERI MOGHANLO**

Student ID: 10712942
Advisor: GIOVANNA SONA
Co-advisor: GIOVANNA VENUTI
Academic Year: 2022-23

Abstract

Salt lakes are interior aquatic ecosystems that are either isolated from the sea or were once connected to it but dried out before being re-flooded by non-marine sources. Increased agricultural activities, water depletion, drought, diversion, upstream water competition, and other anthropogenic activities are all factors that contribute to Salt Lakes depletion. Urmia lake is one of Iran's most important lakes and the second-largest Salt Lake in the world. The lake has suffered catastrophic desiccation since 1995 and its trend has only been decreasing. when a significant decline in lake level began.

The purpose of this project is change detection of Urmia lake surface water from 2018 to 2022 by using Landsat 8-9 OLI/TIRS C2 L2 satellite images and QGIS. Different classification methods were used to classify the study area. Minimum distance, maximum likelihood, spectral angle mapping and random forest were four classification methods were used during this study. Minimum distance and spectral angle mapping results were more acceptable and were chosen as the classification methods. Therefore, classified maps were developed in four categories: water, salt, urban area and bare soil collectively, and vegetation. Then change maps were created year by year. According to the results, the water surface increased from 2018 to 2019 and then decreased from 2018 to 2022. Minimum distance and spectral angle mapping methods show a reduction of 17% and 27% in water surface from 2018 to 2022.

Key-words: Change detection, Lake Urmia, Surface water, Landsat

Abstract in Italian

I laghi salati sono ecosistemi acquatici interni che sono isolati dal mare o un tempo erano collegati ad esso ma si sono prosciugati prima di essere nuovamente allagati da fonti non marine. L'aumento delle attività agricole, l'esaurimento dell'acqua, la siccità, la deviazione, la competizione idrica a monte e altre attività antropogeniche sono tutti fattori che contribuiscono all'esaurimento dei laghi salati. Il lago Urmia è uno dei laghi più importanti dell'Iran e il secondo lago salato più grande del mondo. Il lago ha subito un catastrofico prosciugamento dal 1995 e la sua tendenza è solo in calo. quando iniziò un significativo calo del livello del lago.

Lo scopo di questo progetto è il rilevamento del cambiamento delle acque superficiali del lago Urmia dal 2018 al 2022 utilizzando immagini satellitari Landsat 8-9 OLI/TIRS C2 L2 e QGIS. Diversi metodi di classificazione sono stati utilizzati per classificare l'area di studio. Distanza minima, massima verosimiglianza, mappatura dell'angolo spettrale e foresta casuale sono stati quattro metodi di classificazione utilizzati durante questo studio. I risultati della mappatura della distanza minima e dell'angolo spettrale erano più accettabili e sono stati scelti come metodi di classificazione. Pertanto, le mappe classificate sono state sviluppate in quattro categorie: acqua, sale, area urbana e suolo nudo collettivamente e vegetazione. Quindi le mappe di cambiamento sono state create anno dopo anno. Secondo i risultati, la superficie dell'acqua è aumentata dal 2018 al 2019 e poi è diminuita dal 2018 al 2022. I metodi di mappatura della distanza minima e dell'angolo spettrale mostrano una riduzione del 17% e del 27% della superficie dell'acqua dal 2018 al 2022.

Parole chiave: Rilevamento del cambiamento, Lago Urmia, acque superficiali, Landsat

Contents

1 Introduction

1.1. Motivation and object

One of the main reasons lakes are viewed as delicate landscape features is because they have always been impacted by climatic changes. Lakes are one of the most vital ecosystems for meeting human needs and one of the most potent forces influencing environmental change.(Malahlela, 2016)

The shortage and crises of water resources, particularly in arid and semi-arid countries, is one of today's top issues. Monitoring is an essential part of managing water resources, including lakes, rivers, and dam reservoirs. For environmental monitoring and management, surface water change modelling and mapping in lakes, rivers, and reservoirs are crucial issues. Even though they are quite accurate, conventional in situ measurements have the drawbacks of being fairly expensive and having a low level of spatial and temporal resolution. Remote sensing (RS), while if less precise, can significantly help to mitigate these problems. Time series RS data provide precise information regarding the meteorological, environmental, and socio-economic impacts of lake water change, which can be used to complement in situ monitoring.(Schmidt, Gonda and Transiskus, 2021)

Urmia lake is one of Iran's most important lakes and the second-largest Salt Lake in the world.(Karbassi *et al.*, 2010) that was among the greatest overly salty lakes in the world formerly, but in recent years, its surface area has been decreasing. The United Nations Educational, Scientific, and Cultural Organization (UNESCO) recognized it as a biosphere reserve in 1975 because it is a significant ecological and geo-tourism zone. Unfortunately, 35 dams on 21 rivers that drain into Lake Urmia have been built recently to support agricultural growth in the area. Nonetheless, the lake has been in a perilous situation lately because of a decrease in surface water and an increase in salinity. Because of the reliance of agriculture on river irrigation canals in the Lake Urmia basin, Lake Urmia water levels have decreased recently.(Hesami and Amini, 2016)

the objectives of this study are:

1- Determining the best classification method among minimum distance, maximum likelihood, spectral angle mapping and random forest methods
2- detecting of the surface changes in Urmia lake year by year from 2018 to 2022.

1.2. State of the art

1.2.1. Environmental impacts of Salt Lake

Water is made available to industrial, domestic, irrigation, and environmental sectors by reservoirs, wetlands, and lakes(Duan and Bastiaanssen, 2013). Lakes serve as an essential ecosystem and inland water resource that control climate, document environmental changes, and preserve ecological balance and biodiversity (Mammides, 2020). Lakes' ecological health and sustainability have been seriously threatened since the early 20th century due to rapid urbanization, global climate change, and high anthropogenic activity(Ho and Goethals, 2019).

The functionality of a category of lakes that are more saline, Salt Lakes, are not considered as a resource for potable or agricultural purposes but these lakes and associated wetlands provide breeding habitat for different species, mineral resources, recreational accommodation (Frank and Conover, 2017) .

Salt lakes are interior aquatic ecosystems that are either isolated from the sea or were once connected to it but dried out before being re-flooded by non-marine sources (Williams, 2002). The total volume covered by saline lakes on Earth is 104,103 km3 (44% of total volume and 23% of total surface area). With salinities greater than 3 g/L, geographically widespread saline lakes are an important part of the inland aquatic ecosystem (Messager et al., 2016, p. 13603).

The origin and evolution of saline lakes were caused by volcanic, tectonic, and glacial activities primarily in semi-arid and arid climate regions on Earth (Waiser and Robarts, 2009). The chemical composition of saline differs from that of freshwater lakes that are enriched with cations (Na and Cl) and (CO3)2-/HCO3 with a Ca2+, Mg2+, and SO42- dominance (Hardie, Smoot and Eugster, 1978). In figure 1 Global distribution of saline lakes and reservoirs on world map is shown.

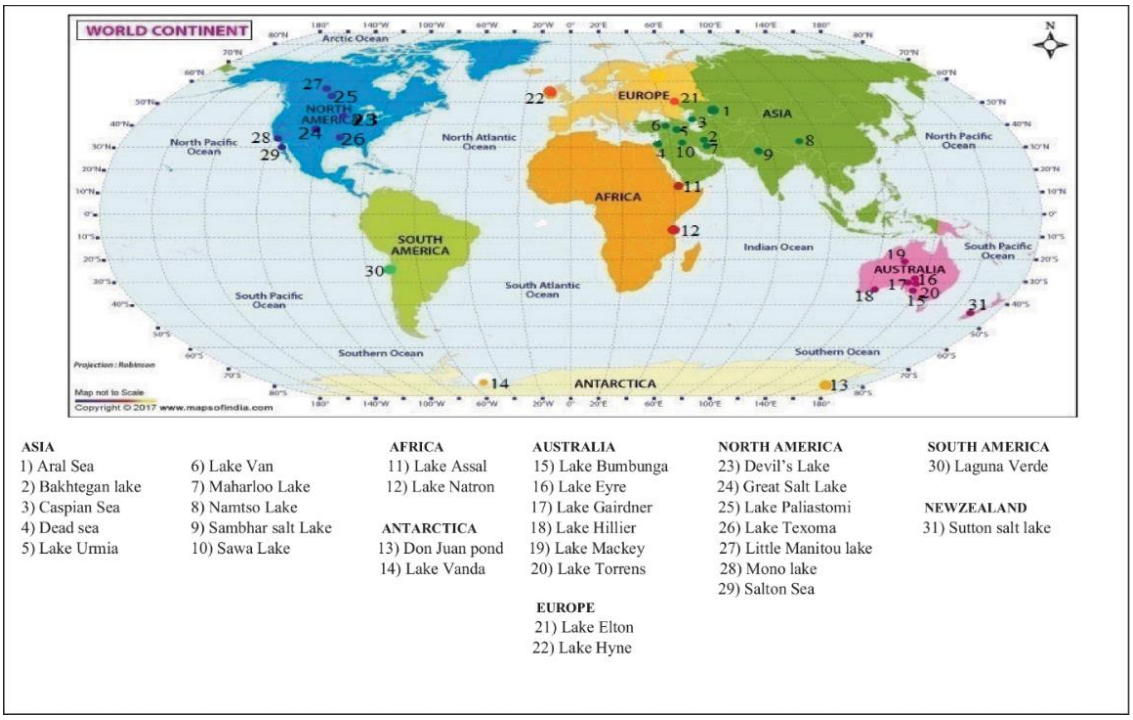

Figure 1:Global distribution of saline lakes and reservoirs on world map(Yechieli and Wood, 2002)

Their immense importance to avian communities makes them designated as Ramsar sites (a wetland site designated to be of international importance under the Ramsar Convention) or Western Hemispheric Shorebird Reserve sites (a science-based, partnership-driven, conservation initiative for protecting the ecological integrity of critical habitats for shorebirds throughout the Americas) such as Lake Urmia in Iran; Great Salt Lake in North America; Sambhar Saline Lake in India and Lakes Nakuru and Bogoria in Kenya (Wurtsbaugh et al., 2017).

1.2.1.1. Benefits of salt lakes

The ecological, socioeconomic, and economic benefits of saline lakes are numerous, but not easily quantifiable. Terminal saline lakes can accumulate and recycle nutrients better than freshwater systems (Blomqvist, Gunnars and Elmgren, 2004), these ecosystems, such as the hyposaline Aral Sea, produce large amounts of food for fish. When salinities are too high for fish to survive, invertebrate food organisms are only available to birds at the top of the food chain. Millions of migratory shorebirds and waterfowl use saline lakes for nesting and to fuel long migrations with abundant food resources such as brine shrimp (Artemia spp.) and brine flies (Ephedra spp.). When saline lakes are desiccated, the amount of habitat decreases and salinities can rise above the tolerance of these invertebrates, limiting both food and habitat for birds (Roberts, 2013).

Similar to freshwater systems, saline lakes are also important for recreational activities. Many saline lakes are popular for swimming, boating, fishing, birdwatching, and

waterfowl hunting. Many of these uses are reduced or eliminated as a result of lake desiccation. Access to lakes becomes difficult when waters retreat across broad playas and marinas become distant from the water's edge (Bioeconomics, 2012).

Mineral extraction is a major economic benefit of salt lakes. Increasing salinity can benefit these industries by concentrating minerals. In severe cases, however, waters recede far from solar evaporation ponds, or complete desiccation eliminates the source of easily accessible brine (Barnes and Wurtsbaugh, 2015).

Harvesting brine shrimp resting eggs (cysts) is another multimillion-dollar industry in saline lakes, but these organisms do not reproduce well at salinities above 200 g/L (Agh et al., 2008). For example, the near-complete desiccation of Lake Urmia increased salinity above 350 g/L and wiped out brine shrimp, resulting in the extinction of flamingos and other birds (Lotfi, 2012).

1.2.1.2. Reason of water reduction in Salt Lakes

According to previous studies, in recent years, these valuable and vital ecosystems are declining at an alarming rate. Numerous lakes in dry and semiarid regions have shown trends in declining water levels and decreasing water area brought on by climatic change (Kraemer et al., 2020). This phenomenon affects the life system in and around the Lakes (da Costa et al., 2016).

Global warming has impacted the physical, chemical, and biological properties of lakes, as well as affected regional distribution and rainfall intensity (Malahlela, 2016). Increased agricultural activities, water depletion, drought, diversion, upstream water competition, and other anthropogenic activities are all factors that contribute to Salt Lakes depletion (Schulz et al., 2020). Typically, lake water level regimes are seen as a key indicator of the water budget of lake systems, which is influenced by watershed hydrological processes (such as precipitation, runoff production, and evapotranspiration) and water allocations made by people (Woolway et al., 2020).

One of saline reservoirs that is the focus of this study, Urmia Lake, with an area of up to 6000 km2, was once the world's second-largest hypersaline lake. The lake has suffered catastrophic desiccation since 1995 and its trend has only been decreasing. when a significant decline in lake level began. The lake lost 90% of its volume and 60% of its area in 2013 (Schulz et al., 2020).

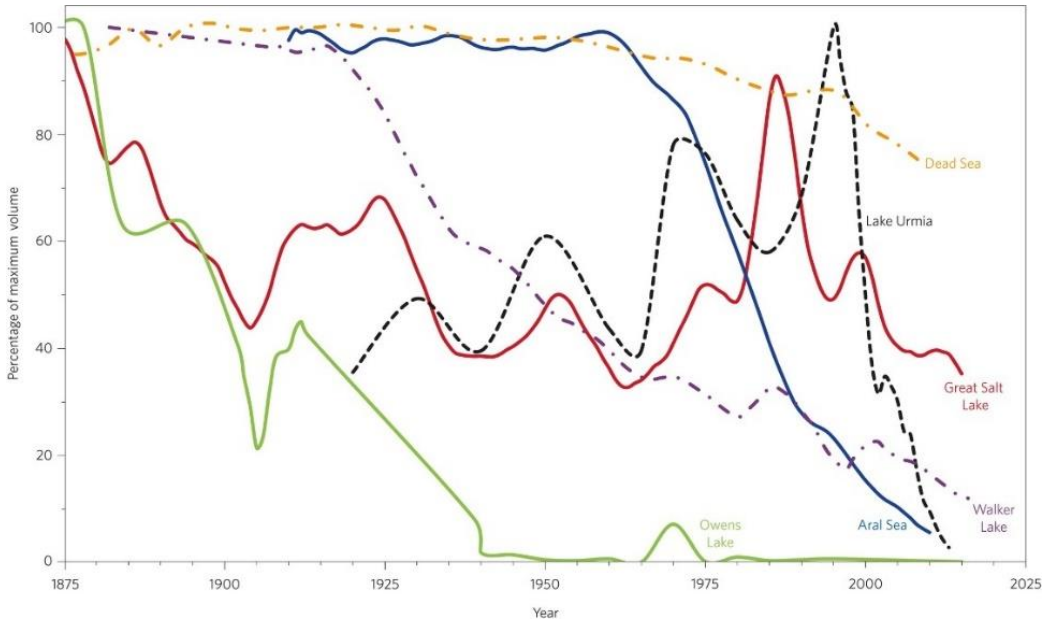

Figure 2:Major decreases in the water volumes of important saline lakes over the past 140 years (Wurtsbaugh et al., 2017)

For the case of Urmia Lake, researchers have investigated the connection between meteorological variables, river discharge, and water level variation. Researchers have also looked into how human activities, such as the expansion of agriculture in the basin, and climate change are contributing to the lake's dropping water level (Sattari et al., 2020). Like all salt lakes, due to its high salt content, the water is not suitable for use in agriculture, hence environmental considerations are crucial in this situation. Yet there are several freshwater aquifers close to Urmia Lake, and people typically use the water from these sources for irrigation. Overexploitation of nearby aquifers for agricultural use has exacerbated the fall in lake water level as a result of the interaction between the neighbouring aquifer and lake water, which also results in salt water intrusion into the nearby aquifers from the lake (Sattari et al., 2020).

Using the Mann-Kendall and Pearson tests, Fathian et al.(2016) examined the trend of temperature and precipitation in the Urmia Lake basin as well as the correlations between temperature, precipitation, and streamflow trends. The results show that, the streamflow is more susceptible to temperature variations than to changes in precipitation, according to the correlation studies between streamflow and climatic factors.

Nourani, et al.(2018). looked into the patterns of rainfall, streamflow, temperature, and humidity in the Urmia Lake basin and examined how these factors interacted with changes in water level throughout the years from 1971 to 2013. The findings revealed significant declining patterns in the lake water level and streamflow series, a moderate descending trend in the rainfall and relative humidity series and increasing trends in the observed temperature data.

According to Dariane et al., (2019) Urmia Lake's water level is falling due to an increase in temperature, a decrease in river input, and only a limited number of major negative trends in precipitation. They also stated that the key factor contributing to the current Urmia Lake catastrophe is the rising agricultural water use. Subsequent research found that the reduction of Urmia Lake's water has a substantial impact on the region's climate.

Using the help of remote sensing data, ground observations, and a hydrological model, (Chaudhari et al., 2018) examined how changes in the climate and those brought on by humans affected the variance in water levels in Urmia Lake. According to their findings, between 1987 and 2016, the amount of agricultural land increased by 98% and the amount of urban land increased by 180%, respectively. The lake area shrunk by 86% as a result. Two simulations, one with and one without human activities, compared the river inflow with the lake, and the results showed that, between 1995 and 2010, human water management activities decreased streamflow by 1.74 km3/year, which is equivalent to 86% of the total loss in lake volume over the same time period. Also, it was discovered that the need for irrigation water nearly tripled, leading to significant river withdrawals. Their findings showed that significant anthropogenic changes to land use, streamflow, and water storage within the basin are also to blame for the continued depletion of Urmia Lake, in addition to long-term droughts.

To understand the causes of the desiccation of Urmia Lake, (Khazaei et al., 2019) looked at the relationships between changes in the hydrological (soil moisture, and water level), vegetation cover (including agricultural crops and other vegetation), and atmospheric climate change (precipitation, temperature). Their findings demonstrated that the dramatic drop in lake water level after 2000 cannot be attributed to precipitation, temperature, or soil moisture changes. However, the shift in the lake's water level is well correlated with the agricultural growth in vegetation cover in the watershed, pointing to this human-driven vegetation cover and concomitant irrigation extension as the primary human cause of the desiccation of Urmia Lake. Moreover, the watershed's runoff into the lake has diminished, and the lake's remaining, lower inflow has not been enough to maintain the prior lake’s water level, causing the observed water level drop to current conditions.

1.2.1.3. Hazards

When saline lakes become severely desiccated, they become sources of fine dust that harms human health and agriculture (Micklin, 2007). for instance, due to agricultural water withdrawals in Aral Sea 12,700 km2 of lakebed was exposed (Indoitu et al., 2015). Airborne dust in Owens Lake, California, has frequently exceeded US air-quality standards for large particulate particles PM10 and increased the prevalence of asthma, lung infections and other respiratory diseases in nearby area (Kittle, 2000).

1.2.1.4. Solutions

To preserve saline lakes, two approaches have been used. The first is the 'Aral Sea solution,' in which the lake area, and thus the evaporative surface, is artificially reduced to match the reduced discharge into the lake (Micklin, 2016). For the Aral Sea, a 13-km-long dike was constructed in 2005 to reach the optimistic scenario of the future Aral Sea (after 2030) as shown in figure 3.

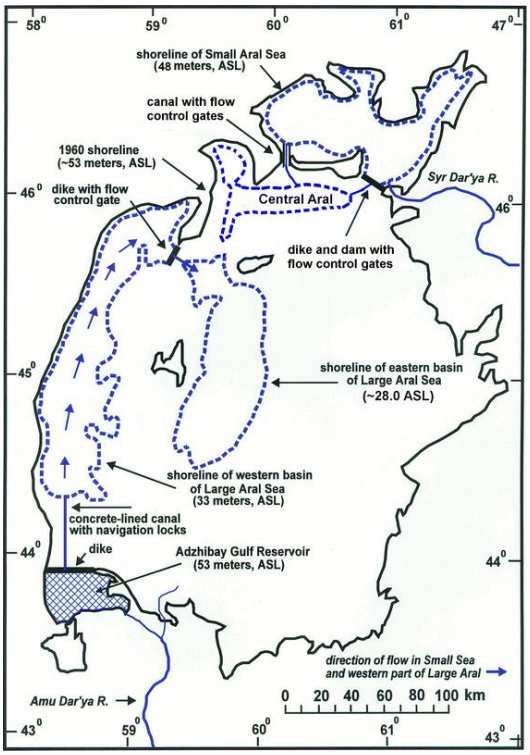

Figure 3:Optimistic scenario of the future Aral Sea (after 2030)(Micklin, 2016)

This action preserves a small hyposaline lake about 5% the size of the former lake, despite the fact that the remaining 95% of the lake area is hypersaline or dry, and salt-dust storms continue to harm crops and human health (Micklin, 2016). Other lakes, such as Lake Urmia and Great Salt Lake, have existing transportation causeways that could be used to manage lake levels and salinity (Lotfi, 2012; White, Null and Tarboton, 2015). However, the cost of constructing a smaller lake, as well as the loss of ecosystem services and the costs of mitigating dust impacts, must be considered when weighing the tradeoffs between water withdrawals and lake area reduction (Wurtsbaugh et al., 2017).

A second option for preserving saline lakes is to estimate and prosecute the minimum water delivery required to keep them alive. This strategy presupposes increased water conservation or water transfers (Wurtsbaugh et al., 2017). For example, when minimum stream flows into California's Mono Lake were litigated under the Public Trust Doctrine in 1994, the Los Angeles metropolitan area lost 12% of its water supply, which was offset by substantial water conservation. With improved water use efficiency, Los Angeles water use has remained relatively constant due to improved

water use efficiency (Ryan, 2015). A pipeline and diversion from an adjacent watershed have also been proposed to help raise water levels in Iran's Urmia Lake (Lotfi, 2012) and and Utah's Great Salt Lake basin already receives a small amount of water from the Colorado River Basin via a diversion (Miller, 1987).

Mean annual inflows would need to be increased by approximately 24-29% for Great Salt Lake and Nevada's Walker Lake to maintain lake levels that would protect wildlife, lake access, human health, and other beneficial uses (Null and Wurtsbaugh, 2020). Lake Urmia in Iran would need to increase current lake inflows by approximately 83% to reach 1274 m of depth and salinity of 250 g/L to recover brine shrimp and birds while minimizing dust impacts on agriculture and the human population (Lotfi, 2012).

1.2.2. Remote sensing

Remote sensing provides information about objects on or near the Earth's surface and atmosphere based on radiation reflected or emitted by those objects. Image data is typically captured at a distance from above. Such data allow us to determine the composition and nature of the Earth's surface and atmosphere from local to global scales, as well as assess changes by analyzing images captured at different points in time (Read and Torrado, 2009).

Remote sensing satellites with varying spatial, spectral, and temporal resolutions provide enormous amounts of data that have become primary sources, being extensively used in recent decades for detecting and extracting surface water and its changes (McFeeters, 2013).

The visible, near-infrared, short-wave infrared, mid-wave infrared, thermal infrared, and microwave regions are the major spectral regions used in Earth remote sensing. Remote-sensing imaging instruments can be divided into two classes:

Passive optical remote sensing, Solar radiation is used as an illumination source in sensors such as multispectral and hyperspectral sensors. Its primary spectral regions of interest are the visible, near-infrared, and shortwave infrared. Many satellites with multiple passive sensors onboard are currently flying above our heads, and many more are being built or planned in the coming years.

Active remote sensing uses an artificial source of radiation as a probe, and the signal that returns to the sensor characterizes the atmosphere or the earth. The Synthetic Aperture Radar system works in real time. It can emit radiation in the microwave region from a moving sensor and measure the backscattered component returned to the sensor from the ground (Zhang and Moore, 2014).

Although the majority of passive sensors operate in the visible and infrared portions of the EMS, some passive microwave sensors are also measure a variety of parameters

such as wind speed, atmospheric and sea surface temperature, soil moisture, rainfall, and atmospheric water vapor (Fath, 2018).

Water body extraction is becoming increasingly important in a variety of research fields, including wetlands management, surface water change detection monitoring, and water cover status evaluation (Ouma and Tateishi, 2006). Remote sensing (RS) and geographic information systems (GIS) have been widely used to study and monitor changes in coastal and inland wetlands over time using available multispectral satellite data. These tools enable the extraction of spatial, spectral, and temporal features (Hereher, 2015). Recently, RS and GIS have been used for the computation and analyses of various water indices, allowing for timely monitoring of water bodies based on satellite data availability and assisting in policy and decision-making processes (Verpoorter, Kutser and Tranvik, 2012).

1.2.3. Change detection of salt lakes

One of the most popular applications of remote sensing analysis of landscape transformation processes is change detection, which refers to the process of comparing differences in the features of a specific area or phenomenon over two or more temporal epochs (Hussain et al., 2013). It is a method in which two images taken at different times are classified separately and the results of the two classifications are compared (Lillesand, Kiefer and Chipman, 2015). For this application, the primary source of data is geographic and is typically in digital (e.g., satellite imagery), analog (e.g., aerial photos), or vector (e.g., feature maps) format. Ancillary data (for example, historical, economic, and so on) can also be used. (Singh, 1989).

Change Detection using remote sensing technology is widely used in a variety of applications, including land use/cover change, disaster monitoring, forest and vegetation change, urban sprawl, and hydrology (Rokni et al., 2014). Reliable information on the spatial distribution of open surface water is critical in many scientific disciplines, including the assessment of current and future water resources, climate models, agricultural suitability, river dynamics, wetland inventory, watershed analysis, surface water survey and management, flood mapping, and environmental monitoring (Sun et al., 2012).

Several image processing techniques for extracting water features from satellite data have been developed in recent decades. To extract water features, single-band methods use a predetermined threshold value. Errors are common in this type due to the mixing of water pixels with those of different cover types (Du et al., 2012). For improved surface water extraction, multi-band methods combine different reflective bands. Surface water change detection is typically accomplished by extracting water features individually from multi-date satellite images before comparing them to detect changes (Du et al., 2012). The vast information in multispectral images can be extracted in change detection research using various image processing techniques such as

spectral mixture analysis, machine learning-based classification, artificial neural networks (ANN), spectral unmixing based methods (Onyango and Opiyo, 2022).

Spectral index-based approaches are the most common and widely used of these techniques since they are easy to perform and produce reliable results. They are created by combining data from multiple bands of a multispectral image to improve delineation accuracy (Polykretis, Grillakis and Alexakis, 2020).

2 Materials and methods

2.1. Study area

Urmia Lake is a lake that can reach 140 km in length from north to south and 85 km in width from east to west during times of high water in Iran's northwest, inside the Urmia Lake Basin.(Vaheddoost et al., 2015) Three provinces of West Azerbaijan, East Azerbaijan, and Kurdistan of Iran share the Urmia Lake Basin. It can be categorized as a semi-arid (cold) climate zone because it is situated between 35° 40′ and 38 °30′ East latitudes and 44° 07′ to 47° 53′ North longitudes.(Vaheddoost and Aksoy, 2017) The lake's surface size may have once reached 6100 km2, but since 1995, it has typically been shrinking. In August 2011, satellite data estimated that the lake's surface area was just 2366 km2.(Eimanifar and Mohebbi, 2007)

Figure 4:Geographical localization of Urmia Lake in the northwestern of Iran(Asem et al., 2014)

In this study, August was chosen for change detection in Urmia lake. the lake's condition was visually assessed for each month of the year. Landsat images for three years (from 2020 to 2022) were analyzed. Apendix A figure 48 to 50 show the area of the lake in 2020, 2021 and 2022 in different months. In 2020, from January to July, the water area of the lake has not changed significantly. From July to November, the area has decreased and in December, the area has increased. In 2021, from January to May, the area of the lake has almost increased. It has decreased from May to October. It increased in November and then decreased in December. In 2022, from January to April, the area of the lake has increased. It has decreased from April to November and increased a little in December. According to these analysis, the lake is almost dry in

August and also the amount of clouds in this month is very low, therefore this month is considered as the most suitable month to detect changes and salinization.

2.2. Image pre-processing

Land use and land cover (LULC) maps are frequently created using multi-spectral remote sensing data for a variety of purposes, such as environmental modeling and monitoring of land use and land cover(Knorn *et al.*, 2009). Since 1972, the Landsat program has regularly delivered high-quality multispectral images with medium spatial and temporal resolution of the Earth's surface(Lyu *et al.*, 2018; Yu *et al.*, 2018; Tang *et al.*, 2019).

First, Landsat 8-9 OLI/TIRS C2 L2 of Urmia lake were downloaded from USGS. To prepare the final image for change detection, three images were downloaded for each year (Path:169 Row:034, Path:169 Row:033, Path:168 Row:034). The Images for every year were on the same date (near mid of August) or with a maximum difference of one week. The cloud cover range were between 0 to 10%. The date of the downloaded Images is shown in the table 1.

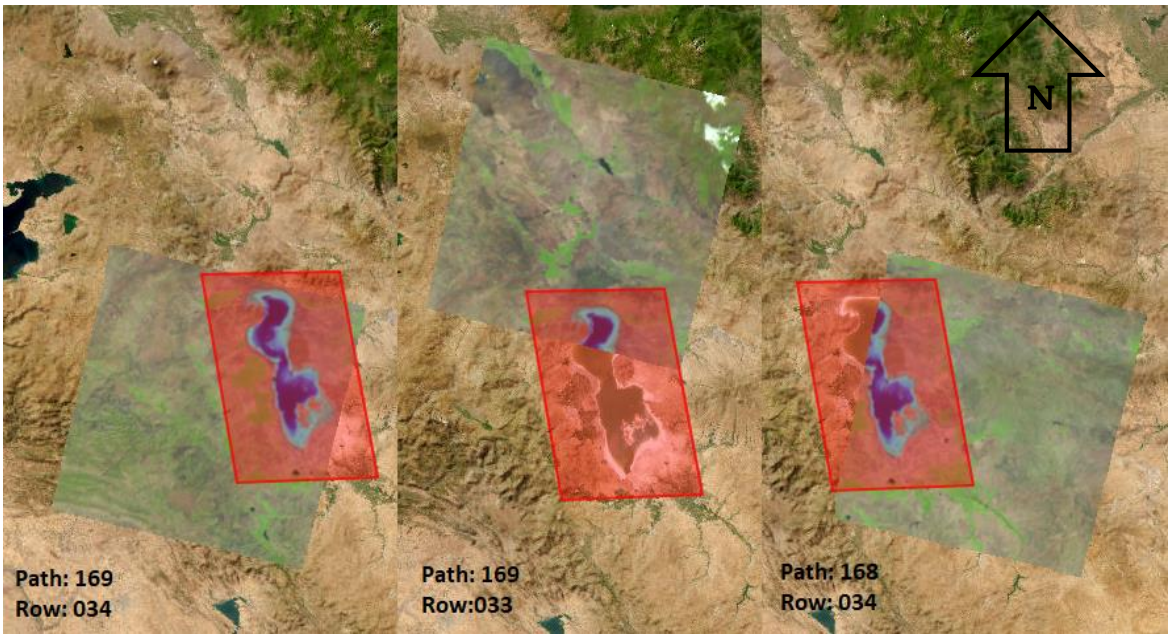

Figure 5:Geographical position of the satellite imageries used for the study area(from left to right: 11/08/2022- 11/08/2022- 12/08/2022)

Table 1:The date of satellite images

Path	169	169	168
Year/Row	**034**	**033**	**034**
2018	2018/08/16	2018/08/16	2018/08/09
2019	2019/08/19	2019/08/19	2019/08/12
2020	2020/08/21	2020/08/21	2020/08/14
2021	2021/08/24	2021/08/24	2021/08/17
2022	2022/08/11	2022/08/11	2022/08/12

An interactive tool called the Spectral Characteristics Viewer can be used to see how the bands, or channels, of various satellite sensors detect the intensity of the various light wavelengths (colors). Also called the relative spectral response, this (RSR). By overlaying the spectral curves from different features (spectra), Which bands on the chosen sensor will function for the application can be determined. (www.usgs.gov)

Table 2:Landsat 8/9 Operational Land Image (OLI) and Thermal Infrared Sensor (TIRS)

bands	Wavelength (micrometers)	Resolution (meters)	Useful for mapping
Band 1 - Coastal aerosol	0.43-0.45	30	Coastal and aerosol studies
Band 2 - Blue	0.45-0.51	30	Bathymetric mapping, distinguishing soil from vegetation and deciduous from coniferous vegetation
Band 3 - Green	0.53-0.59	30	Emphasizes peak vegetation, which is useful for assessing plant vigor
Band 4 - Red	0.64-0.67	30	Discriminates vegetation slopes
Band 5 - Near Infrared (NIR)	0.85-0.88	30	Emphasizes biomass content and shorelines
Band 6 - Shortwave Infrared (SWIR) 1	1.57-1.65	30	Discriminates moisture content of soil and vegetation; penetrates thin clouds
Band 7 - Shortwave Infrared (SWIR) 2	2.11-2.29	30	Improved moisture content of soil and vegetation; penetrates thin clouds

Band 8 - Panchromatic	0.50-0.68	15	15 meter resolution, sharper image definition
Band 9 - Cirrus	1.36-1.38	30	Improved detection of cirrus cloud contamination
Band 10 - Thermal Infrared (TIRS) 1	10.6-11.19	100	100 meter resolution, thermal mapping and estimated soil moisture
Band 11 - Thermal Infrared (TIRS) 2	11.50-12.51	100	100 meter resolution, improved thermal mapping and estimated soil moisture

One of the most used remote sensing datasets for LULC classification is Landsat 8 OLI. As seen in Table 2, Landsat 8 OLI supplied 11 spectral bands. In LULC classification, band 8 through 11 are less frequently used(Yu et al., 2019). In this respect, band 1 to band 7, i.e. coastal, blue, green, red, near-infrared(NIR), shortwave infrared 1(SWIR1), shortwave infrared 2(SWIR2) was selected for analysis.

The images of band1 to band 7 have been opened in QGIS Desktop 3.28.1. and "i.group" tool was used from processing toolbox to group them, in order to use the bands 1 to 7 simultaneously. This function was used to group 7 layers in each section for all years.

Three separate monochrome photographs are frequently combined and each given a specific color; this is known as a color and is helpful composite for photo interpretation(Landsat, 7). Color composites are usually expressed as R G B where:

R stands for Red; G stands for Green; B stands for Blue.

And for Landsat 8 images:

4 is the band number associated to the Red color;

3 is the band number associated to the Green color;

2 is the band number associated to the Blue color.

For converting the images to RGB, the Symbology was changed. In band rendering part, band 4 was set as the red band. Band 3 was set as the green band. Band 2 was set as the blue band. The same was applied to the other sections and the rest of the years.

Figure 6:RGB for Path 169 and Row 034 in August 2022

Then “merge” tool was used to combine 3 grouped images. So by using this tool a single ‘layer’ was obtained for each year.

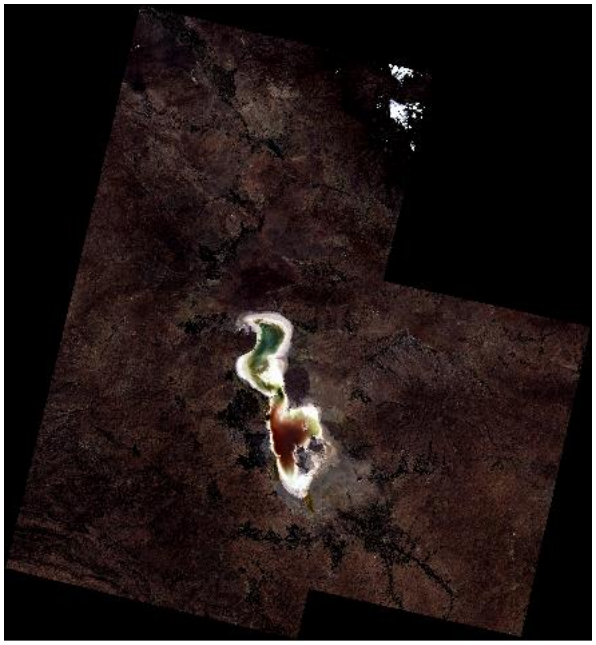

Figure 7:merged in August 2022

The merged image was cut by using a vector to restrict the area of analysis in order to detect the changes in the lake and close a certain surrounding environment. One vector was created and then by using “clip raster by mask layer”, the images was cut. The blue area in Figure 8 is the analysis area in this study. In figure 9, the image ready for doing further steps and classification is shown.

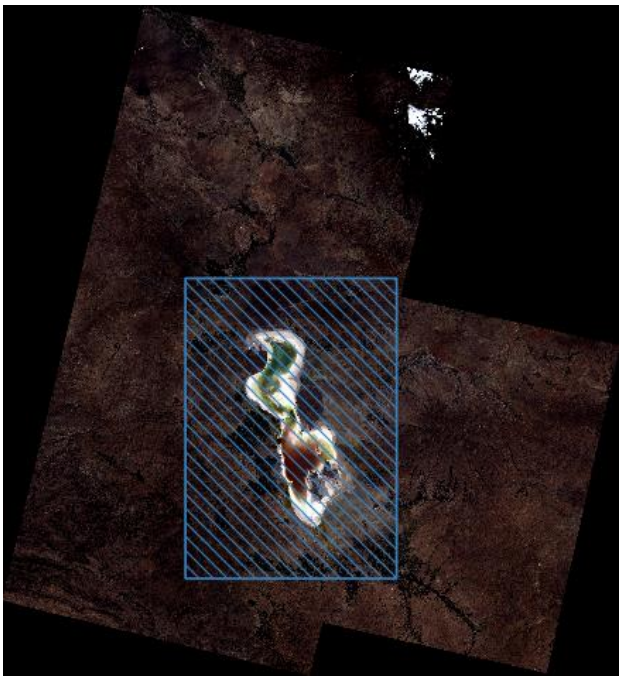

Figure 8:analysis area

Figure 9:preprocessed image in year 2022

The same method was used to prepare the images for the rest of the years. Below are the prepared images.

Figure 10:preprocessed image in year 2021

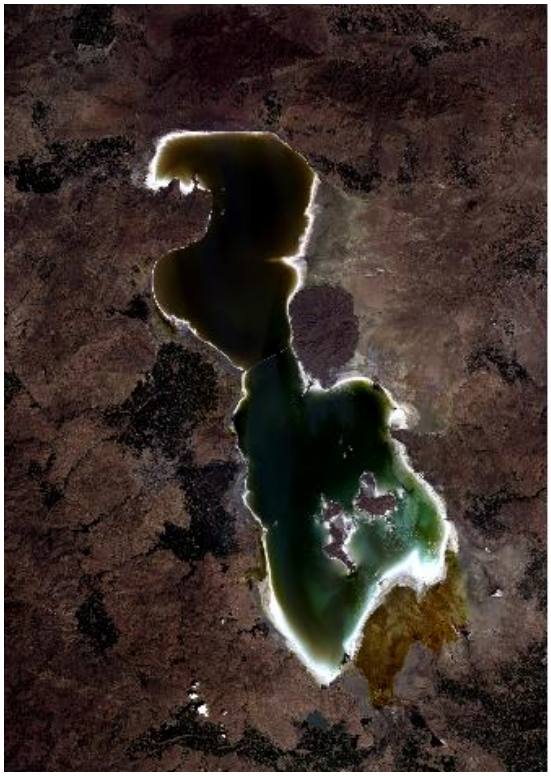

Figure 11:preprocessed image in year 2020

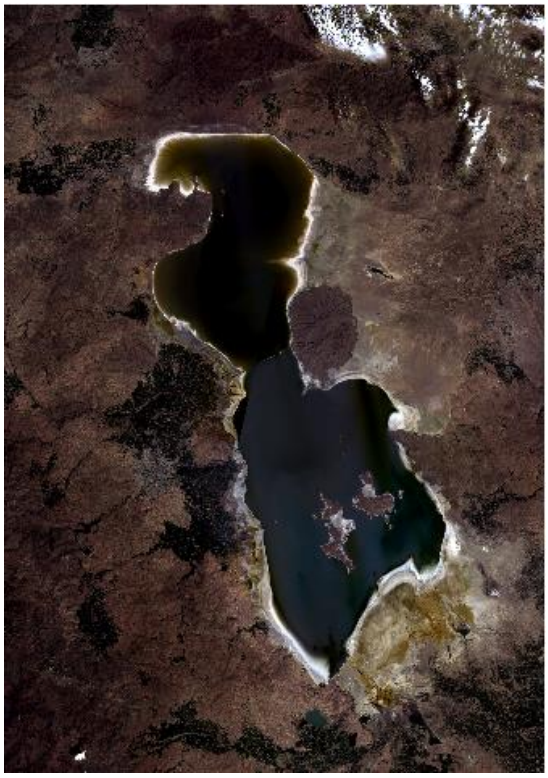

Figure 12:preprocessed image in year 2019

Figure 13:preprocessed image in year 2018

2.2.1. Cloud masking

After the pre-preparation of the images, the images that had clouds were prepared and the clouds were removed. For this purpose, “Cloud masking for Landsat products” plugin was used.

CloudMasking is a Qgis plugin for make the masking of clouds, cloud shadow, cirrus, aerosols, ice/snow and water for Landsat (4, 5, 7, 8, 9) products using different process and filters such as Fmask, Blue Band, Cloud QA, Aerosol and Pixel QA.(https://smbyc.github.io/CloudMasking/)

Some clouds were observed in the years 2019 and 2021. First, Landsat Metadata File(MTL) was opened. The steps were carried out according to figure 14.

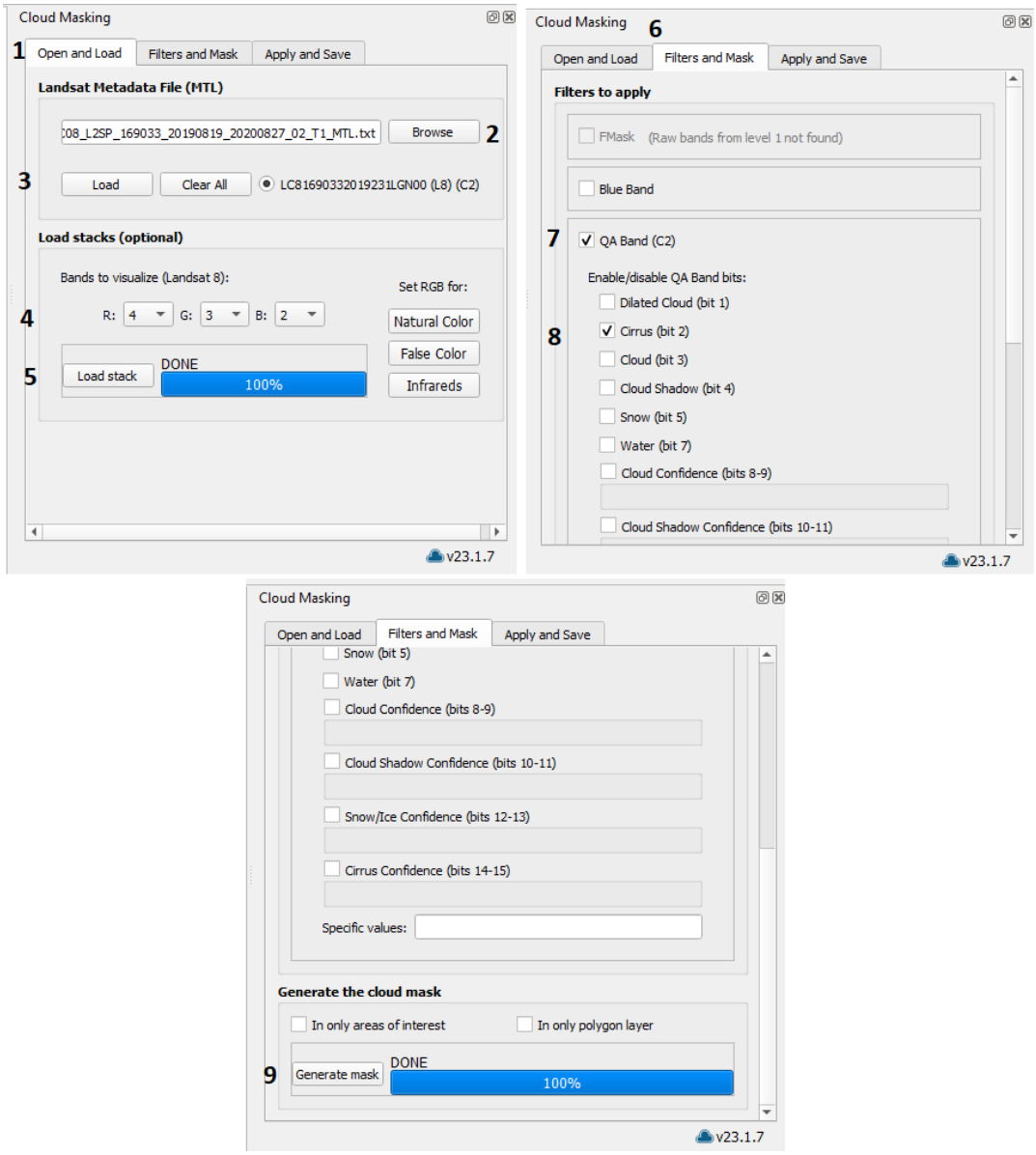

Figure 14: the steps in "Cloud masking for Landsat products" plugin for generating mask to cloud masking

Then save as a GeoTIFF file and do the same procedure for 3 images (Path:169, Row:034 and Path:169, Row:033 and Path:168, Row:034) of each year. Then "merge" tool was used. By using the "clip raster by mask layer" tool, the area of analysis was prepared for next steps. Figure 15 shows the images with 2 values 1 and 10(black:1 and white:10) that 10 refers to the clouds.

Figure 15: clouds in analysis area in year 2019

In this step, "r.null" tool was used twice, first 1 value(black part without cloud) was set to NULL and second 10 value(white part with cloud). By using "Polygonize (raster to vector)" tool, these two raster layers were converted to vector. Using Figure 12 as the "Input layer" in "clip raster by mask layer" tool and vector file which 10 is NULL was set as the "Mask layer". In this image the cloud part value is zero.

Figure 16:image without cloud in year 2019(value of black area is zero)

For cloud part, first the next Landsat 8-9 OLI/TIRS C2 L2 Images of Urmia lake which is around two weeks later were downloaded and all pre-processing steps for the previous images were applied exactly to these images(table 3) as well. Then using new prepared image as the "Input layer" in "clip raster by mask layer" tool and vector file which 1 is NULL was set as the "Mask layer". In this image the without cloud part value is zero. The result is shown in the figure 17. It should be noted that in this figure, the white parts are non-zero and the black parts are zero.

Table 3:The date of satellite images for producing images without cloud in year 2019

Path	**169**	**169**	**168**
Year/Row	**034**	**033**	**034**
2019	2022/09/04	2022/09/04	2022/08/12

Figure 17:image with only the data in cloudy part of Augest 2019(value of black area is zero)

By using “raster calculation”, 7 bands of image 16 and 17 were added together one by one and then converted into one images with “i.group” tool. As a result, the image without clouds for 2019 is shown in figure 18.

Figure 18:preprocessed image in year 2019 without clouds

This method was used to remove clouds because the clouds are not over the lake and the cloud area has not changed much in terms of coverage over the two weeks. The same method was used for 2021.

Figure 19:preprocessed image in year 2021 without clouds

2.3. Classification

In this study "The Semi-Automatic Classification Plugin" and "dzetsaka" were used for classification.

The Semi-Automatic Classification Plugin is a Python plugin for the software QGIS, with the general goal of facilitating land cover monitoring by individuals whose primary field is not precisely remote sensing but that could profit from remote sensing analysis. The Semi-Automatic Classification Plugin offers a set of integrated tools and a user interface for simplifying and automating the land cover classification processes, from downloading remote sensing images to preprocessing (tools for setting up data for analysis or other calculations), processing (tools for performing land cover classification or analysis), and post processing. (i.e. tools for assessing the classification accuracy, refining the classification, or integrating additional data) (Congedo, 2021).

dzetsaka is one of the classification tools in QGIS (developed in 2016(Karasiak and Perbet, 2018)) that allows the user to classify images with several machine learning algorithms(Potić and Potić, 2017).

2.3.1. unsupervised classification

In a multispectral image, clustering is the process of grouping pixels based on their computed spectral similarity (e.g., Euclidean distance or Spectral Angle)(Richards and Jia, 2006).

In this study, in order to get an overview of the different classes in the images, an unsupervised classification method is preliminary used.

K-means and ISODATA are the algorithms offered by SCP (semi-automatic classification) for the various types of clustering, most of which are based on iterative techniques. The ISODATA (Iterative Self-Organizing Data Analysis Technique) method is similar to K-means but with the extra stages of combining clusters with comparable spectral signatures and separating clusters with too much variability (i.e. standard deviation) in spectral signatures(Ball and Hall, 1965).

Image of 2022 was classified by clustering algorithm ISODATA method. Table 4 shows the input information.

Table 4:Input information for unsupervised classification

Description	Input
Distance threshold	0.0001
Number of classes	10
Max number of iterations	10
ISODATA max standard deviation	0.0001
ISODATA minimum class size pixels	10
Seed signatures from band values	Chosen
Distance algorithm	Minimum distance

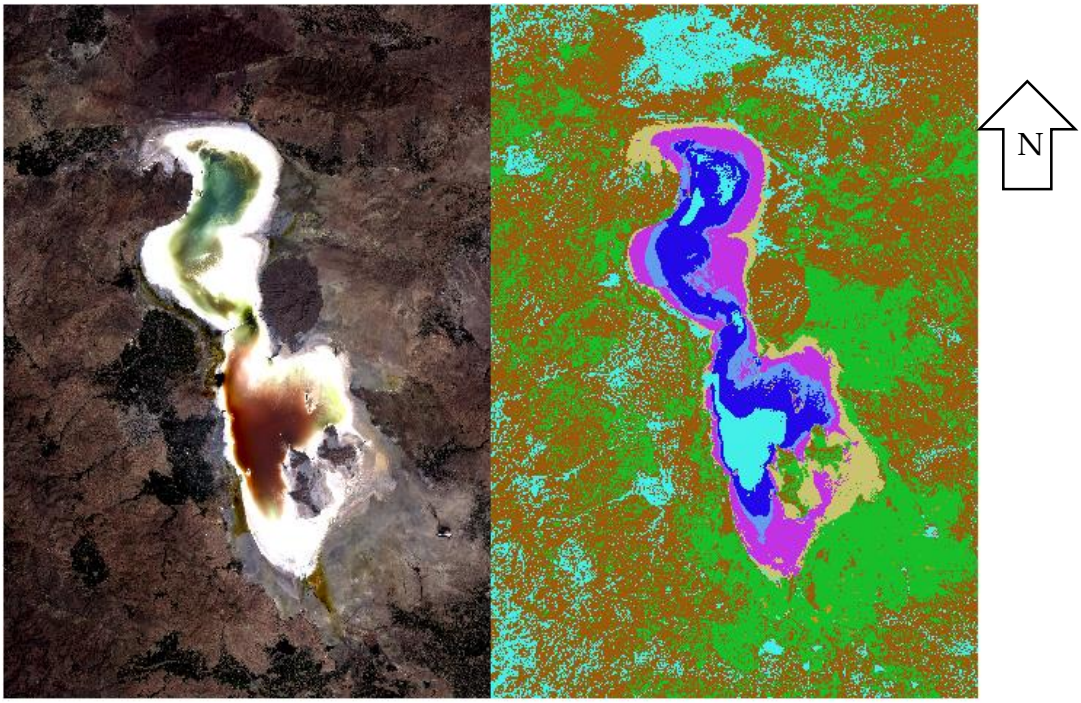

Figure 20: from left to right :analysis area in year 2022 and unsupervised classification in year 2022

According to the Unsupervised Classification and its comparison with the main image, 4 class were considered for classification, including water, salt, vegetation and others. others consist urban area and bare soil.

2.3.2. supervised classification

First, the Semi-Automatic Classification Plugin was used for classification. The images were classified using this plugin with three methods: minimum distance, maximum likelihood, and spectral angle mapping. Second, dzetsaka plugins was used for random forest method.

For each land cover type recognized in the image, supervised classifications usually require the user to choose one or more ROIs (Regions of Interest, also Training Areas). ROIs are polygons that are created over uniform portions of the image and placed over pixels from the same land cover class. An arbitrary ID code can be utilized to identify the various land cover classifications (i.e. Identifier). SCP permits the definition of the identifying codes for land cover classes known as Macro class ID (MC ID) and Class ID (C ID). A Macro class is a collection of ROIs with specified Class IDs that can be used to categorize materials with various spectral signatures that belong to the same land cover class.

In this respect, the clipped image was added in the band set part in SCP window. Then the training sample was created from SCP dock. MC ID s were introduced by creating

ROI polygons. 4 polygons were created for each class (water, salt, urban area and bare soil, vegetation)

For samples of the training area, samples have been tried to be made from different land cover class with different spectral signatures and almost equal size. The attribute table of training sample 2022.

	MC_ID	MC_name	Area
1	1	water	634820
2	1	water	500865
3	1	water	883978
4	1	water	720967
5	2	salt	481502
6	2	salt	609431
7	2	salt	152092
8	2	salt	360360
9	3	urban are and bare soil	48077
10	3	urban are and bare soil	81924
11	3	urban are and bare soil	86698
12	3	urban are and bare soil	652624
13	4	vegetation	26983
14	4	vegetation	81323
15	4	vegetation	76240
16	4	vegetation	44090

Figure 21:attribute table training input sample in year 2022

Figure 22: training sample in year 2022

The reflectance as a function of wavelength is the spectral signature. Each material has an own signature, which can be used to classify the materials(Landsat, 7). Before classification, the spectral signature of the training sample was checked.

After creating training sample, from classification part in band processing by using MC ID and different algorithms (minimum distance, maximum likelihood, and spectral angle mapping) each image was classified 3 times with SCP plugin and one time (Random forest) with dzetsaka plugin.

To classify the images and change detection, 2022 and 2018 were classified first, so that by checking the results, the best classification method was used also for 2019, 2020 and 2021.

2.3.2.1. minimum distance

The following equation describes how the Minimum Distance algorithm determines the Euclidean distance d(x,y) between the training spectral signatures and the spectral signatures of image pixels:

$$d(x,y) = \sqrt{\sum_{i=1}^{n}(x_i - y_i)^2} \qquad \text{Equation 1}$$

where:

x = spectral signature vector of an image pixel;

y = spectral signature vector of a training area;

n = number of image bands.

Therefore, the distance is determined for each individual pixel in the image, and the class of the closest spectral signature is assigned using the following discriminant function.

$$x \in C_k \Leftrightarrow d(x, y_k) < d(x, y_j) \forall k \neq j \quad \text{Equation 2}$$

where:

C_k = land cover class k;

y_k= spectral signature of class k;

y_j= spectral signature of class j.

It is possible to specify a threshold T_i that will prevent pixels below it from being classified:

$$x \in C_k \Leftrightarrow d(x, y_k) < d(x, y_j) \forall k \neq j$$

and

$$d(x, y_k) < T_i \quad \text{Equation 3}$$

(Richards and Jia, 2006).

SCP plugin was used to classify with minimum distance method. The prepared image to classify was opened in band set part in multiband image list section then the "minimum distance" algorithm was chosen from classification section of band processing.

2.3.2.2. maximum likelihood

For determining whether a pixel belongs to a land cover class, the maximum likelihood algorithm calculates the probability distributions for the classes in relation to the Bayes' theorem. In particular, multivariate normal models are used to assume the form of the probability distributions for the classes(Richards and Jia, 2006). This approach can only be used if each training area has an adequate number of pixels to calculate the covariance matrix. According to Richards and Jia (2006), the discriminant function is constructed for each pixel as follows:

$$g_k(x) = \ln p(C_k) - \frac{1}{2}\ln | \sum k | - \frac{1}{2}(x - y_k)^t \sum_k^{-1} (x - y_k) \quad \text{Equation 4}$$

where:

C_k = land cover class k;

x= spectral signature vector of an image pixel;

$p(C_k)$= probability that the correct class is C_k;

$|\sum k|$= determinant of the covariance matrix of the data in class C_k;

Σ_k^{-1}= inverse of the covariance matrix;

y_k= spectral signature vector of class k.

Therefore:

$$x \in C_k \Leftrightarrow g_k(x) > g_j(x) \forall k \neq j \quad \text{Equation 5}$$

In addition, a threshold can be specified for the discriminant function to keep pixels below it from being classified. Considering a threshold T_i the classification condition becomes:

$$x \in C_k \Leftrightarrow g_k(x) > g_j(x) \forall k \neq j$$

and

$$g_k(x) < T_i \quad \text{Equation 6}$$

(Richards and Jia, 2006)

For maximum likelihood method, the same procedure like minimum distance method was done. The only different was choosing the "maximum likelihood" as algorithm.

2.3.2.3. spectral angle mapping

The Spectral Angle Mapping determines the spectral angle between the training spectral signatures and the spectral signatures of the picture pixels. The definition of the spectral angle is:

$$\theta(x,y) = \cos^{-1}\left(\frac{\sum_{i=1}^{n} x_i y_i}{\left(\sum_{i=1}^{n} x_i{}^2\right)^{\frac{1}{2}} * \left(\sum_{i=1}^{n} y_i{}^2\right)^{\frac{1}{2}}}\right) \quad \text{Equation 7}$$

Where:

x= spectral signature vector of an image pixel;

y = spectral signature vector of a training area;

n = number of image bands.

A pixel therefore belongs to the class with the lowest angle, which is:

$$x \in C_k \Leftrightarrow \theta(x, y_k) < \theta(x, y_j) \forall k \neq j \quad \text{Equation 8}$$

where:

C_k = land cover class k;

y_k = spectral signature of class k;

y_j = spectral signature of class j.

It is possible to define a threshold T_i to remove pixels below this value from the classification.

$$x \in C_k \Leftrightarrow \theta(x, y_k) < \theta\left(x, y_j\right) \forall k \neq j$$

and

$$\theta(x, y_k) < T_i \qquad \text{Equation 9}$$

(Kruse *et al.*, 1993)

For spectral angle mapping method, similar to the pervious method was done. "spectral angle mapping" as algorithm was chosen.

2.3.2.4. random forest

Random forests are a combination machine learning algorithm. They are merged with a number of tree classifiers, each of which cast a unit vote for the most popular class; the final sort result is then obtained by merging these results(Liu, Wang and Zhang, 2012).

For classification with random forest method, dzetsaka plugins was used. After adding the main clipped image to classify, the SCP training sample was exported as a vector and then added as ROI in dzetsaka dock. That means, the same as the training sample in 3 previous methods was used in this step. MC_ID was column name where class number was stored.

2.4. Validation and accuracy assessment

In order to evaluate the quality of maps developed from remotely sensed data and to identify and measure map errors, after the classification process, the accuracy of land-use or land-cover classification is necessary. Choosing a sample of locations (pixels) from the study region using a statistically sound sampling design is a common strategy for accuracy assessment. Next, check to see if the land-use or land-cover classification given to each pixel corresponds to the actual classification of the ground location represented by that pixel. It is presumed that the reference categorization, whether it was gained through a ground visit or photointerpretation, is accurate. Several statistical analyses are then performed on the error matrix created from the sample data. The development of an error matrix, which is a table that contrasts map information with reference data (i.e. ground truth data), is typically used to assess accuracy for a number of sample areas(Congalton, Oderwald and Mead, 1983).

Table 5:Scheme of Error Matrix

	Ground truth 1	**Ground truth 2**	**…**	**Ground truth k**	**Total**
Class 1	A_{11}	A_{12}	…	A_{1k}	A_{1+}
Class 2	A_{21}	A_{22}	…	A_{2k}	A_{2+}
…	…	…	…	…	…
Class k	A_{k1}	A_{k2}	…	A_{kk}	A_{k+}
Total	A_{+1}	A_{+2}	…	A_{+k}	N

In this study, since it was not possible to create ground truth sample, a sample was prepared from the main images as a checking sample and the results were compared with it.

In order to validate the results of 2022 and 2018 SCP plugin was used. First a vector file was created as a checking sample (figure 23). It was different from the training sample as shown in figure 22. Five samples were created for each part (water, salt, urban area and bare soil, vegetation). For adding polygon features, the number 1, 2, 3 and 4 were chosen as the ID for water, salt, urban area and bare soil as in same class and vegetation, respectively. The new samples were completely different and far from the previous samples (training sample), and their size were chosen to be almost the size of training samples. In this part, samples were selected from different parts of the image. Then from accuracy window in post processing part in SCP plugins, each classification to assess was selected. The checking sample as the reference vector was selected.

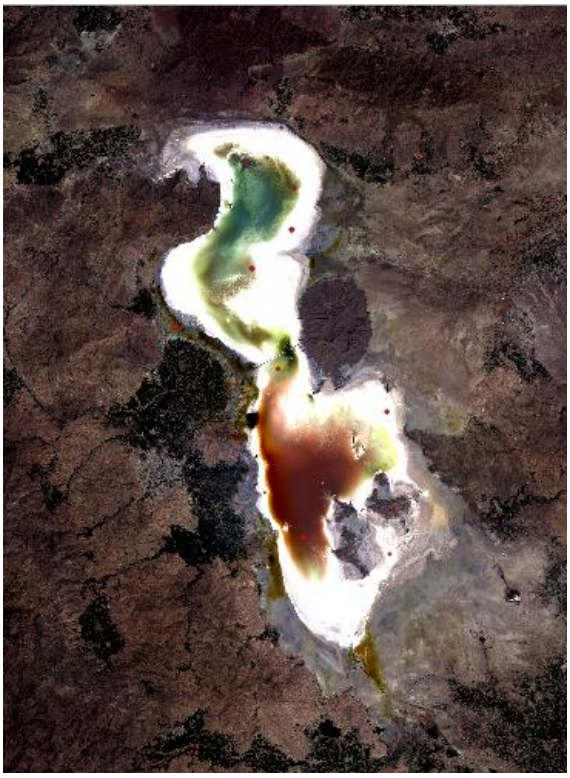

Figure 23:checking sample in year 2022

2.4.1. overall accuracy

As a result, it is possible to determine the overall accuracy as the ratio of the total number of sample units N to the number of samples that are correctly classified (the sum of the major diagonal)(Congalton, 2009).

The overall accuracy is defined as follows (also expressed in percentage):

$$o = \frac{\sum_{i=1}^{k} A_{ii}}{N}$$ Equation 10

2.4.2. kappa index

The kappa coefficient of agreement(Cohen, 1960) is often used to describe the accuracy evaluation results of remote sensing-derived land-use or land-cover classifications(Stehman, 1996). The agreement between two raters who each assign N items to C mutually exclusive categories is measured by Cohen's kappa. the letter K is defined as:

$$k = \frac{P_o - P_e}{1 - P_e} \qquad \text{Equation 11}$$

utilizing the observed data to determine the likelihood of each observer arbitrarily perceiving each category, where P_o is the relative observed agreement among raters and P_e is the hypothetical probability of chance agreement. If the raters are in complete agreement, then kappa =1. If there is no agreement among the raters beyond what can be predicted by chance (as indicated by P_e), Kappa = 0. If there is no correlation between the ratings of the two raters, the statistic could be negative by chance, or it could indicate a genuine propensity for the raters to assign different ratings(Sim and Wright, 2005).

2.4.3. user accuracy

The proportion between the number of accurate samples and the row total is used to determine the user's accuracy for each class (also expressed in percentage):

$$u_i = \frac{A_{ii}}{A_{i+}} \qquad \text{Equation 12}$$

(Congalton, 2009)

2.4.4. producer accuracy

The proportion of correct samples to the column total determines the producer's accuracy for each class (also expressed in percentage):

$$p_i = \frac{A_{ii}}{A_{+1}} \qquad \text{Equation 13}$$

(Congalton, 2009)

2.5. change detection

For detecting the changes, maps were created by “raster calculator” tool. For calculation of the changing map, 4 was multiplied to the classified map of one year and then minus to the classified map of the year before. Since there were four classified categories, 16 cases are possible for changes. It should be noted that this formula is used to assign a specific number to each case.

In table the numbers were allocated to each case is shown.

Table 6:change of each category from one year to next year

value	description
0	vegetation to water
1	Urban Area and Bare Soil to Water
2	Salt to Water
3	Water to Water
4	Vegetation to Salt
5	Urban Area and Bare Soil to Salt
6	Salt to Salt
7	Water to Salt
8	Vegetation to Urban Area and Bare Soil
9	Urban Area and Bare Soil to Urban Area and Bare Soil
10	Salt to Urban Area and Bare Soil
11	Water to Urban Area and Bare Soil
12	Vegetation to Vegetation
13	Urban Area and Bare Soil to Vegetation
14	Salt to Vegetation
15	Water to Vegetation

Also in this step, the area of each class in each year and the changing area were calculated by “Raster layer unique values report” tool.

3 results and discussion

3.1. spectral signature

spectral signature for training sample 2022 is shown in figure 24. 1(blue color) refers to water, 2(yellow color) refers to salt, 3(brown color) refers to urban area and bare soil and 4(green color) refers to vegetation. Multi-spectral surface reflectance curves in figure 25 is shown to compare with the result and a good competence was observed.

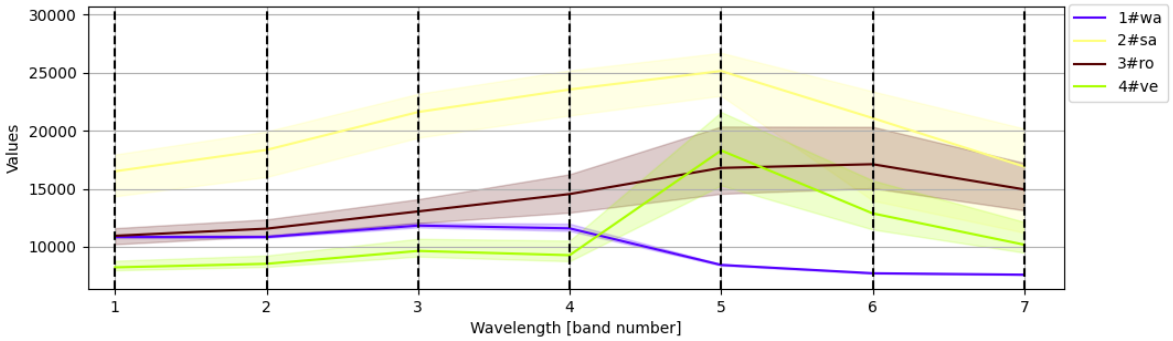

Figure 24:spectral signature – 2022

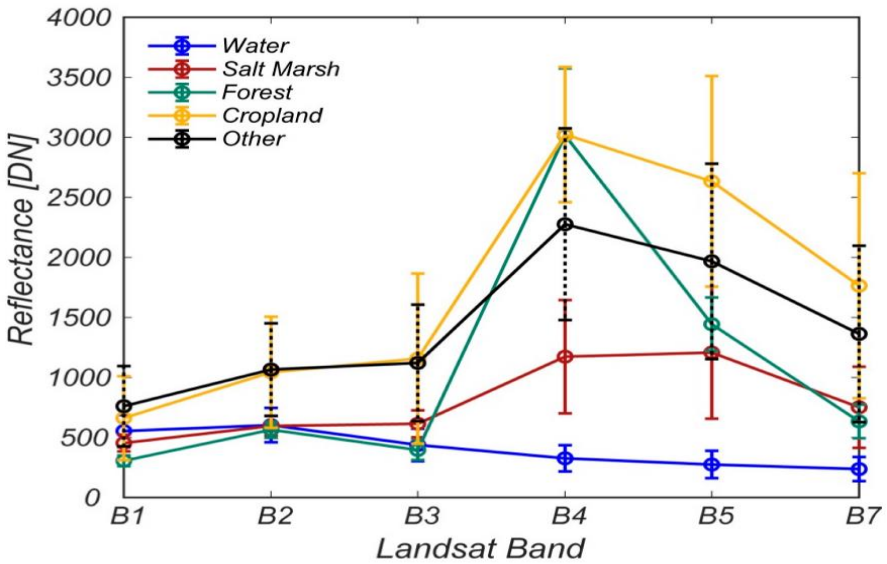

Figure 25:Multi-spectral surface reflectance curves for the five (Fagherazzi *et al.*, 2019).

3.2. classification and validation

The results of classification 2022 by four different methods are shown in figure 26 to 29. The result of minimum distance and spectral angle mapping methods are almost the same or very slightly different from each other. In the case of water and salt, minimum distance, spectral angle mapping, random forest methods are almost the same, but maximum likelihood method is very different from these three methods. As for maximum likelihood method, the water area of the lake has shown much less specially in the southern part of the lake. In the case of random forest method, it has identified a larger area as vegetation than the previous three methods and in this method compared to minimum distance and spectral angle mapping methods, it has identified water and salt as soil in some areas.

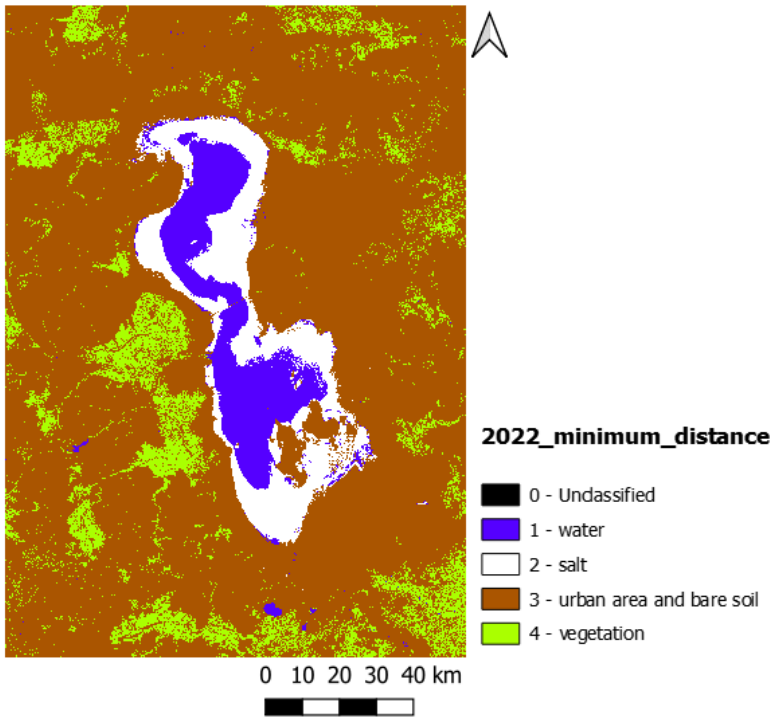

Figure 26: classified map using minimum distance 2022

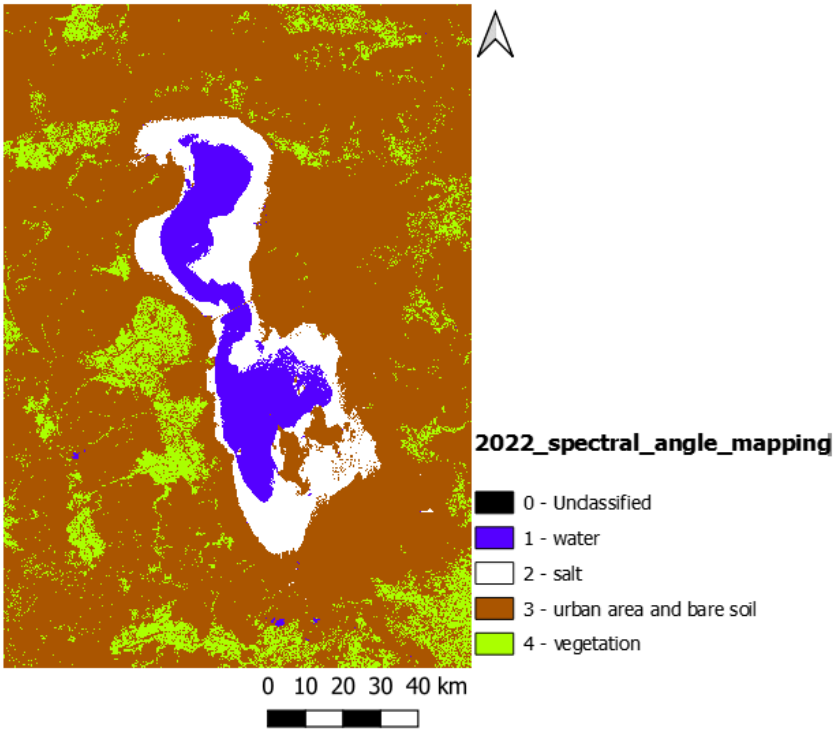

Figure 27: classified map using spectral angle mapping 2022

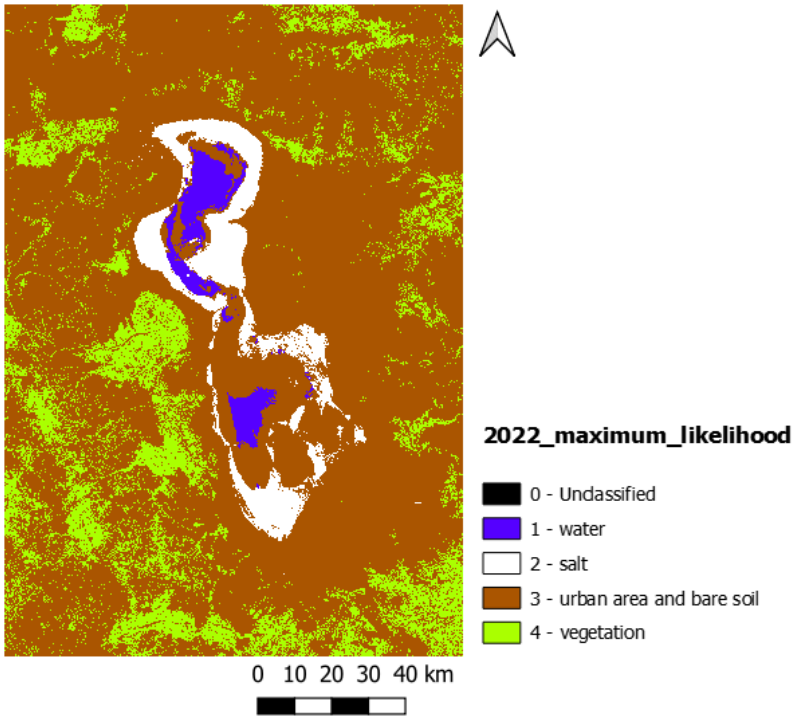

Figure 28: classified map using maximum likelihood 2022

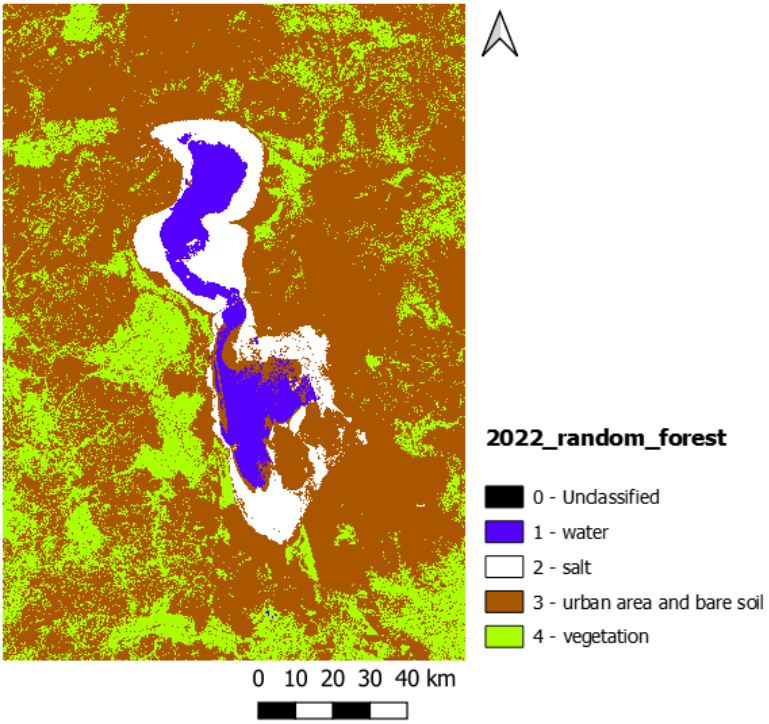

Figure 29: classified map using random forest 2022

The results of classification 2018 by four different methods are shown in figure 30 to 33. Minimum distance and spectral angle mapping methods are approximately the same results. In the case of water and salt in this year, maximum likelihood and random forest are completely different from minimum distance and spectral angle mapping. In maximum likelihood method compared to minimum distance and spectral angle mapping methods, it has identified the water and salt as soil in some areas specially in the southern part of the lake. In random forest method, water is less and salt is more than minimum distance and spectral angle mapping methods. Vegetation is almost the same in 4 methods in 2018.

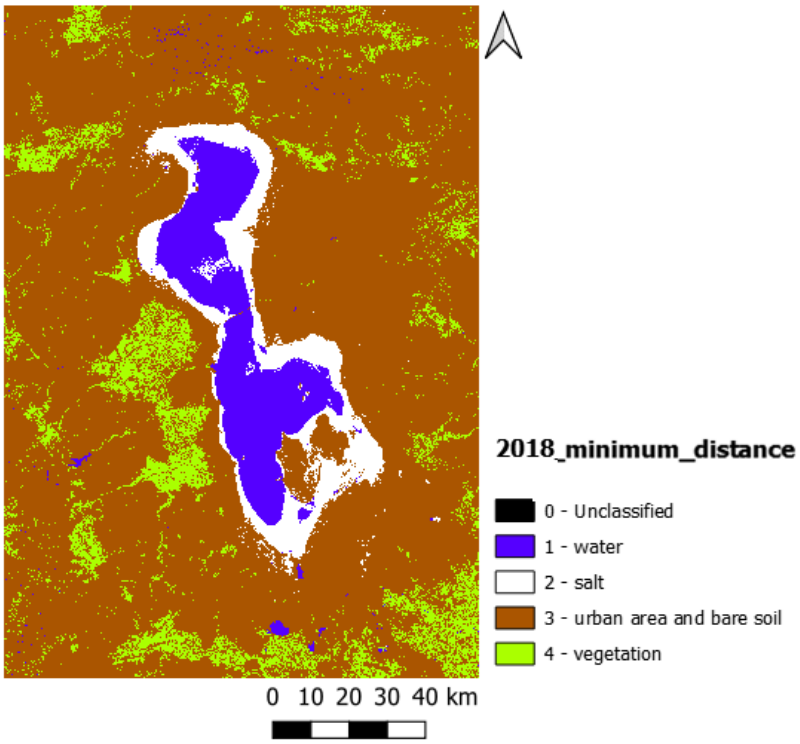

Figure 30:classified map using minimum distance 2018

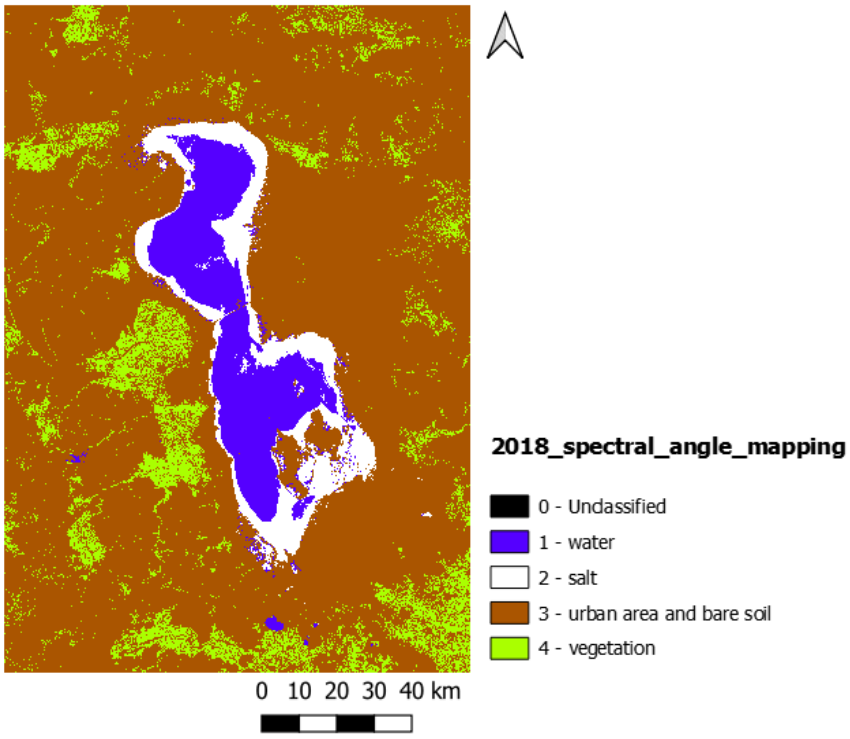

Figure 31: classified map using spectral angle mapping 2018

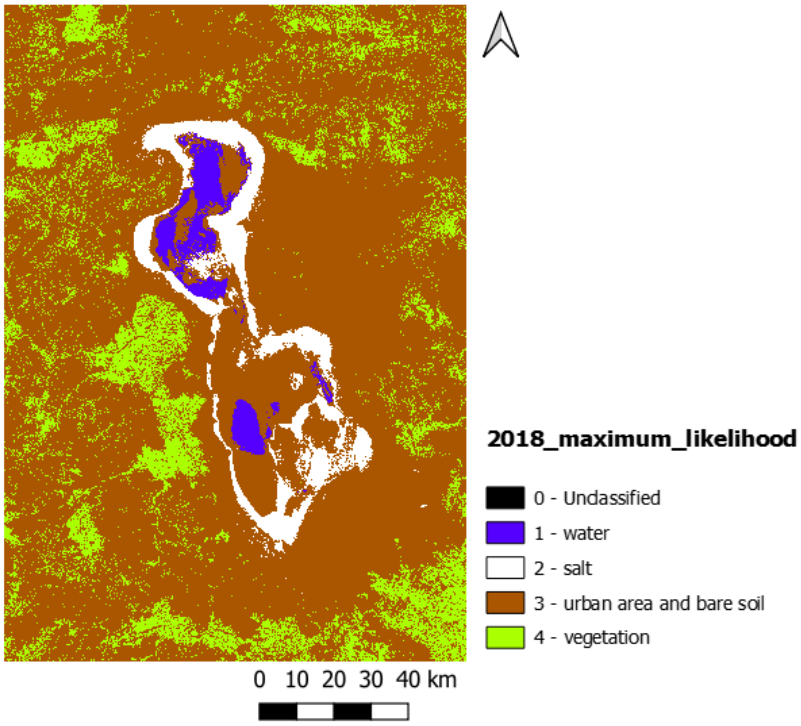

Figure 32: classified map using maximum likelihood 2018

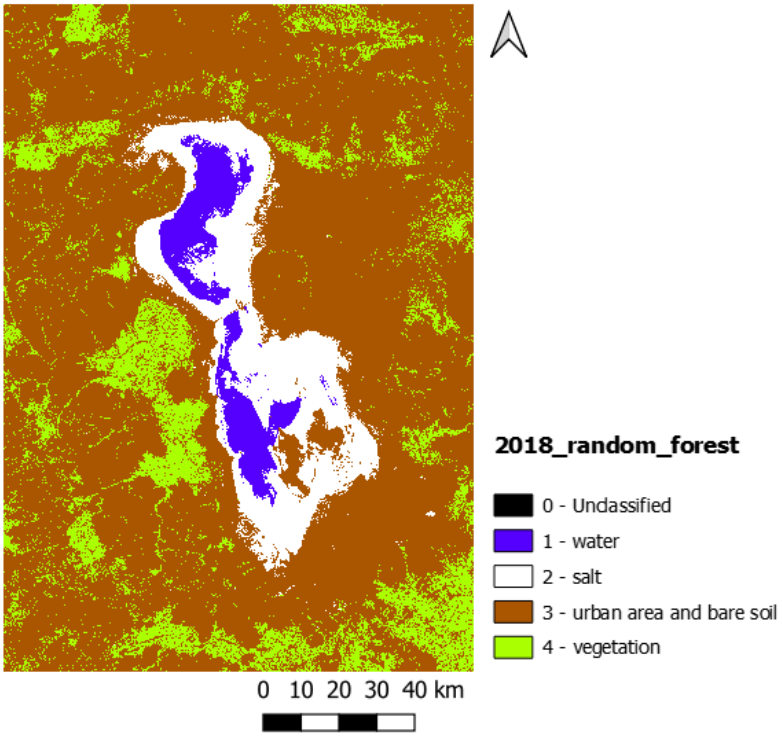

Figure 33: classified map using random forest 2018

The overall accuracy, overall kappa index, producer and user accuracy for the classification results of year 2022 and 2018 are shown in table 7 to 10. The results of minimum distance and spectral angle mapping method in two years were the most accurate. After these two methods, random forest methods have higher overall accuracy. The overall accuracy of 98.84% and 98.66% are the highest overall accuracy that are refer to spectral angle mapping method in 2018 and 2022 respectively.

Table 7: overall accuracy

Year	Minimum Distance	Spectral Angle Mapping	Maximum Likelihood	Random Forest
2018	97.39	98.84	50.96	95.14
2022	98.65	98.66	47.66	73.43

Table 8:kappa hat classification

Year	Minimum Distance	Spectral Angle Mapping	Maximum Likelihood	Random Forest
2018	0.94	0.97	0.33	0.89
2022	0.97	0.97	0.31	0.50

Table 9: producer accuracy

Year	Class	Minimum Distance	Spectral Angle Mapping	Maximum Likelihood	Random Forest
2018	1 - Water	100.00	100.00	4.81	47.86
2018	2 - Salt	76.95	96.55	46.38	100.00
2018	3 - soil	100.00	100.00	100.00	99.88
2018	4 -vegetation	91.62	90.68	97.51	95.30
2022	1 - Water	100.00	100.00	4.09	96.62
2022	2 - Salt	100.00	100.00	54.69	24.87
2022	3 - soil	99.96	99.96	99.85	86.84
2022	4 -vegetation	87.77	88.19	98.67	97.68

Table 10: user accuracy

Year	Class	Minimum Distance	Spectral Angle Mapping	Maximum Likelihood	Random Forest
2018	1 - Water	99.95	99.49	100.00	100.00
2018	2 - Salt	100.00	100.00	100.00	59.39
2018	3 - soil	96.62	98.54	37.18	99.10
2018	4 -vegetation	100.00	100.00	100.00	99.34

2022	1 - Water	100.00	100.00	100.00	10.00
2022	2 - Salt	100.00	100.00	100.00	97.51
2022	3 - soil	98.28	98.28	33.96	74.15
2022	4 -vegetation	99.70	99.70	99.71	56.06

Minimum distance and spectral angle mapping, whose results were very close to each other, were chosen as the chosen method. They were chosen to continue the classification for the years 2019, 2020, and 2021. All the steps to classify the 2019, 2020 and 2021 were completely similar to the classification method in 2022 and 2018. Figure 34 to 39 are the results of classification by two chosen methods for 2019, 2020 and 2021. The results of the years 2020 and 2021 are similar for two methods. But in 2019, especially in salt and soil detection, there is a significant difference between the results of minimum distance and spectral angle mapping methods.

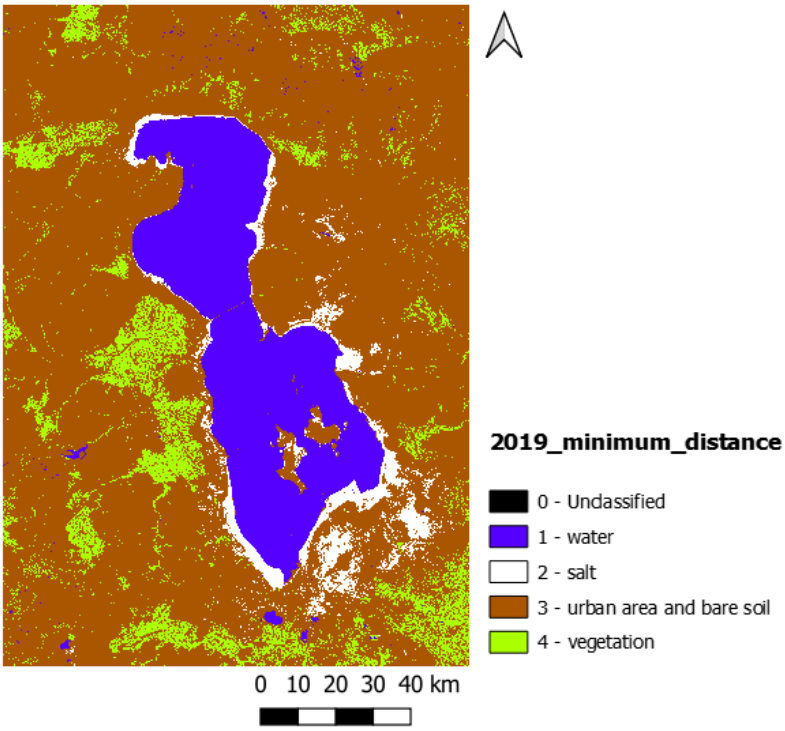

Figure 34: classified map using minimum distance 2019

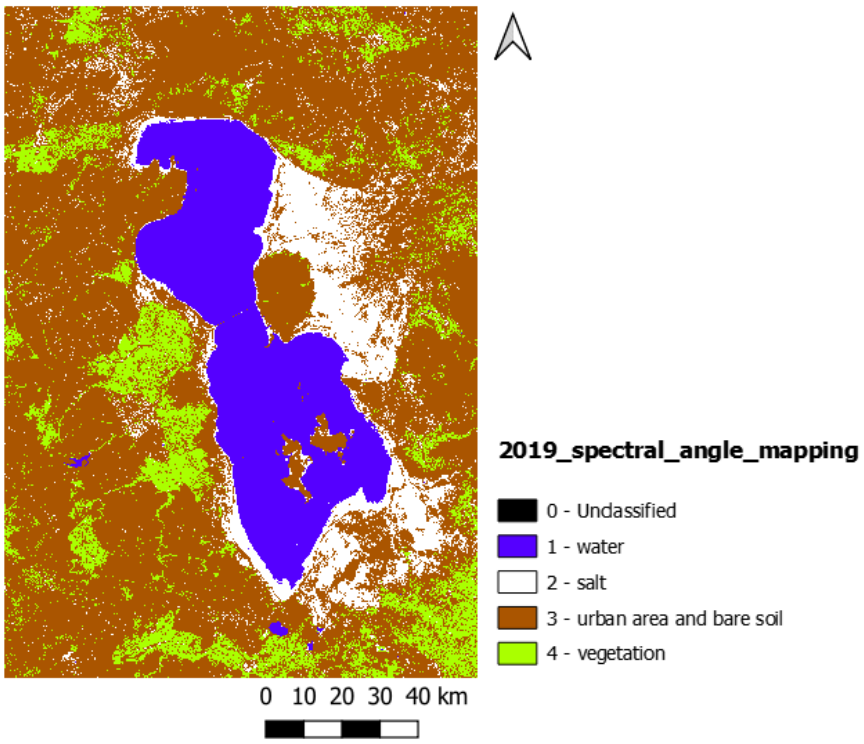

Figure 35: classified map using spectral angle mapping 2019

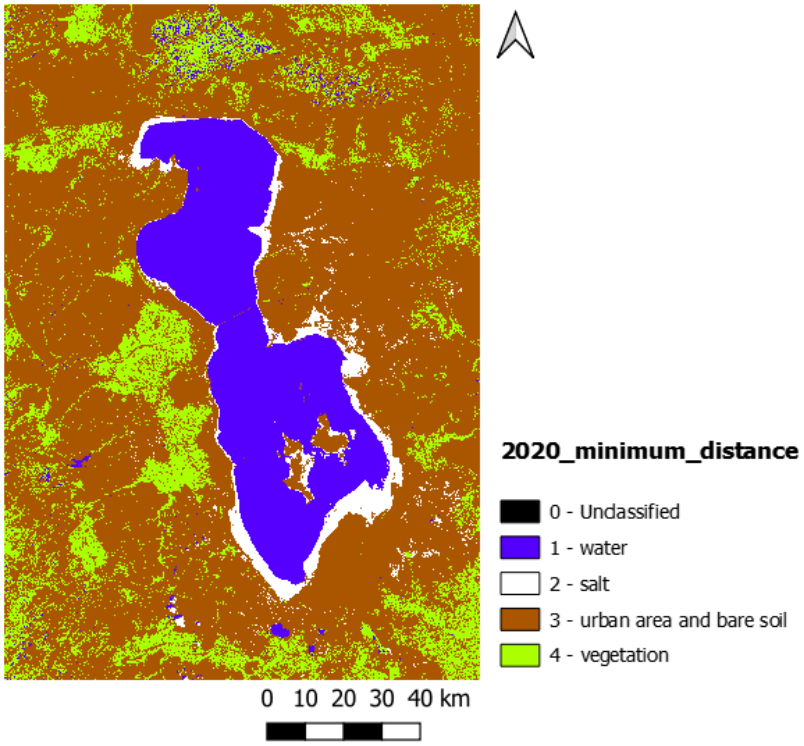

Figure 36: classified map using minimum distance 2020

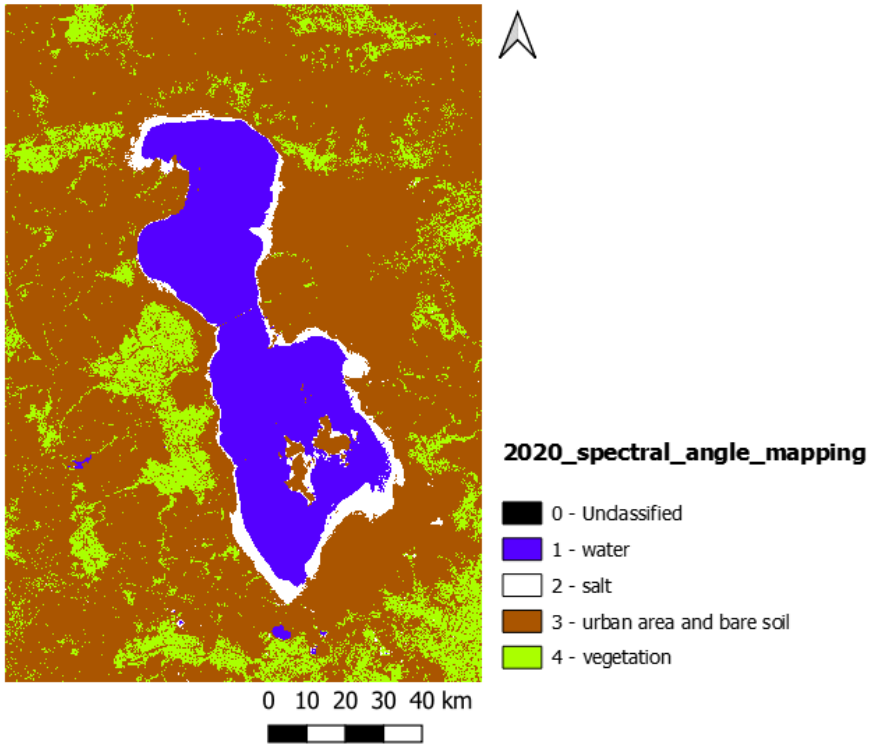

Figure 37: classified map using spectral angle mapping 2020

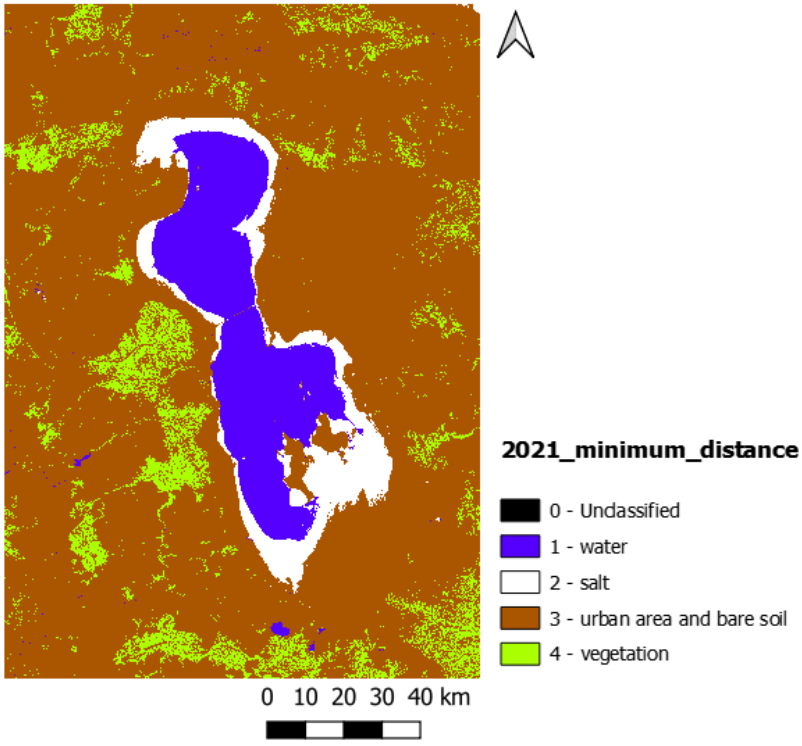

Figure 38: classified map using minimum distance 2021

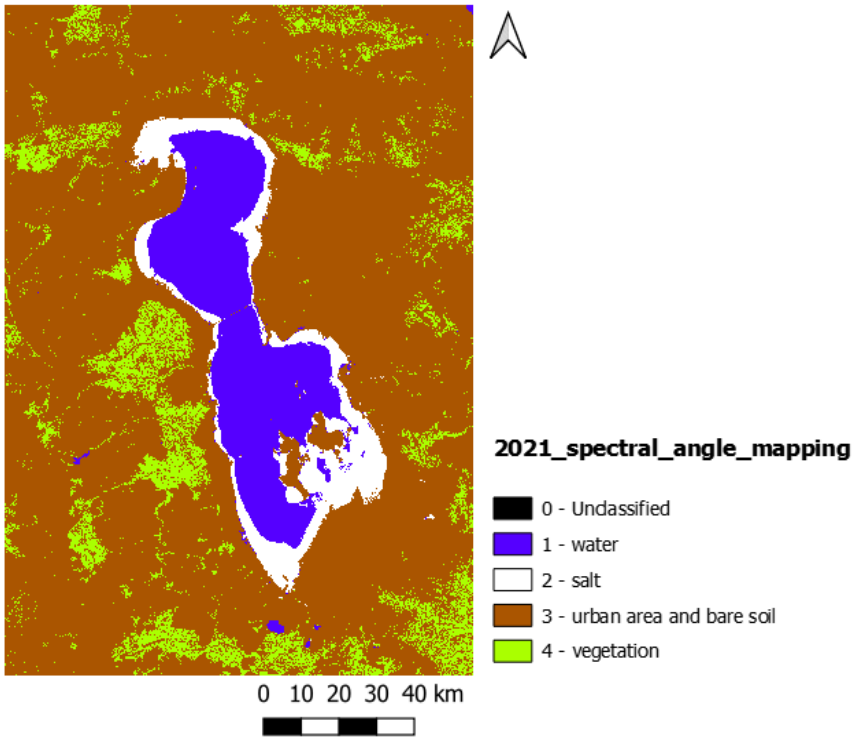

Figure 39: classified map using spectral angle mapping 2021

The results of accuracy assessment of 2019 to 2021 are shown in table 11 to 14. In 2019 and 2021, overall accuracy of minimum distance method is more than spectral angle mapping and they are 98.85% and 97.14% respectively. In 2020, the overall accuracy of spectral angle mapping is more than another and 99.36%.

Table 11:overall accuracy

Year	Minimum Distance	Spectral Angle Mapping
2019	98.85	90.99
2020	99.33	99.36
2021	97.14	96.07

Table 12:kappa hat classification

Year	Minimum Distance	Spectral Angle Mapping
2019	0.97	0.85
2020	0.99	0.99
2021	0.93	0.91

Table 13:producer accuracy

Year	Class	Minimum Distance	Spectral Angle Mapping
2019	1 - Water	100.00	100.00
2019	2 - Salt	100.00	57.84
2019	3 - soil	99.98	98.02
2019	4 -vegetation	88.27	96.47
2020	1 - Water	100.00	100.00
2020	2 - Salt	100.00	98.72
2020	3 - soil	99.98	99.99
2020	4 -vegetation	95.61	95.50
2021	1 - Water	100.00	100.00
2021	2 - Salt	91.48	73.45
2021	3 - soil	99.96	99.96
2021	4 -vegetation	77.89	81.94

Table 14:user accuracy

Year	Class	Minimum Distance	Spectral Angle Mapping
2019	1 - Water	99.95	99.92
2019	2 - Salt	99.86	90.67
2019	3 - soil	98.43	87.28
2019	4 -vegetation	99.87	99.65
2020	1 - Water	99.97	100.00
2020	2 - Salt	99.94	99.97
2020	3 - soil	99.03	99.09
2020	4 -vegetation	99.93	99.95
2021	1 - Water	100.00	82.50
2021	2 - Salt	100.00	100.00
2021	3 - soil	96.30	97.26
2021	4 -vegetation	99.68	99.68

3.3. change detection

The results of classification by minimum distance and spectral angle mapping of previous step were used to create the changing maps that are shown in figure 40 to 47.

Initial letters of words are used in the legend of maps. ‘V’ refers to Vegetation. ‘W’ refers to Water. ‘S’ refers to Salt and ‘UB’ refers to Urban area and Bare soil. In this study, the change of water to salt (W to S) is more desired.

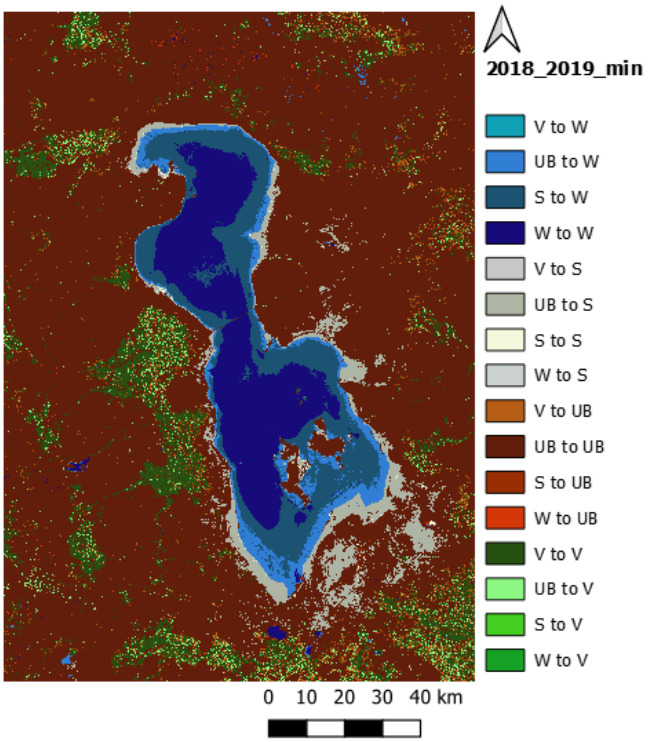

Figure 40: changing map from 2018 to 2019 using minimum distance

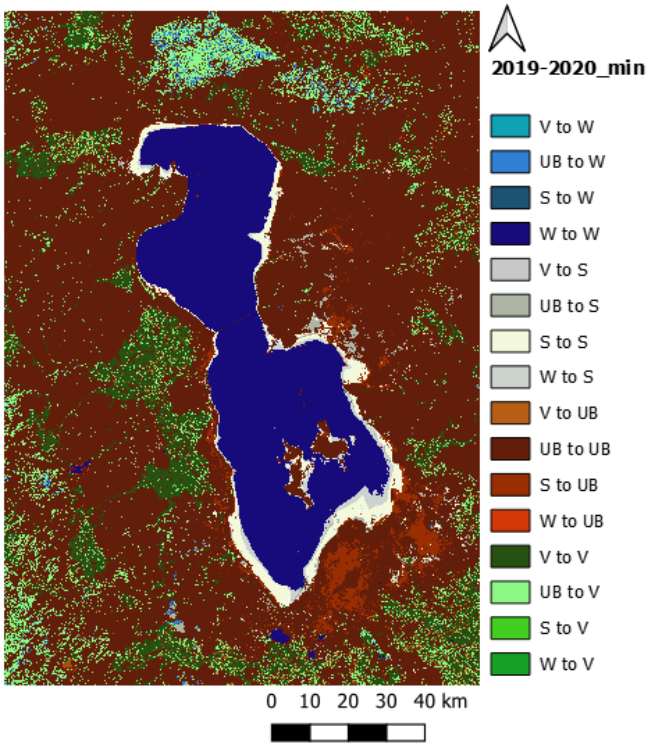

Figure 41:changing map from 2019 to 2020 using minimum distance

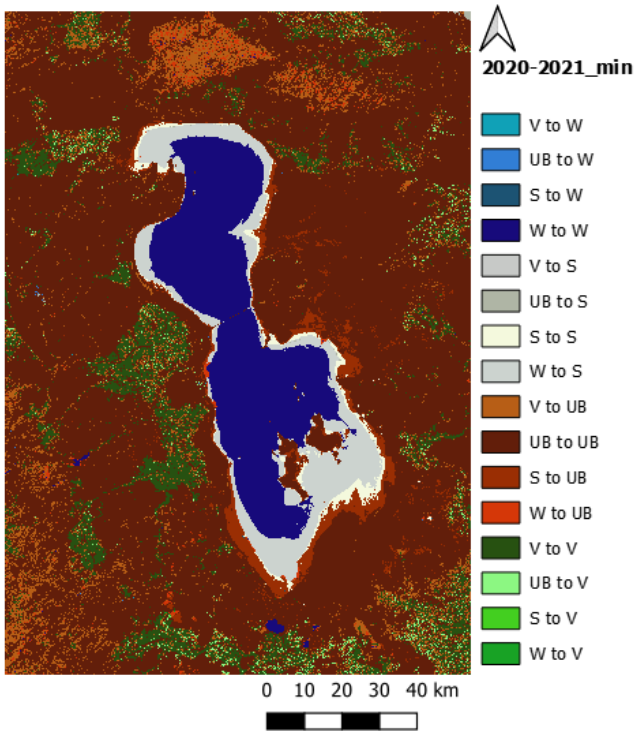

Figure 42:changing map from 2020 to 2021 using minimum distance

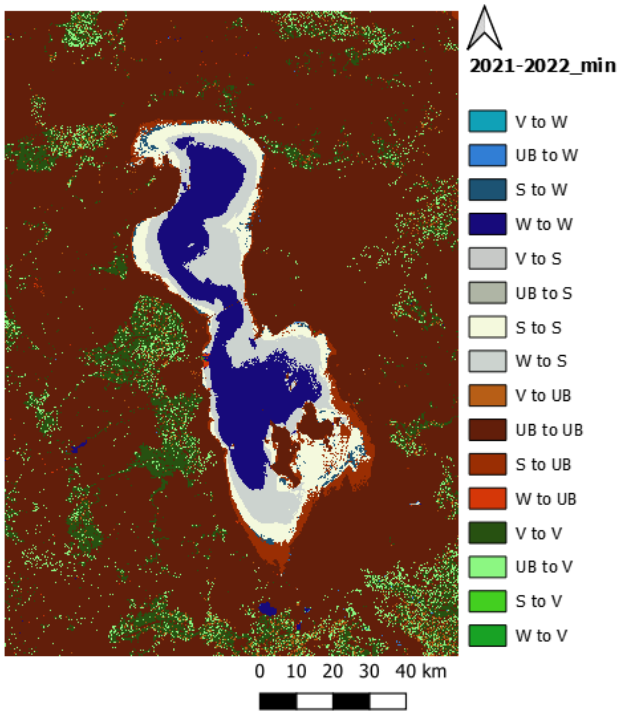

Figure 43:changing map from 2021 to 2022 using minimum distance

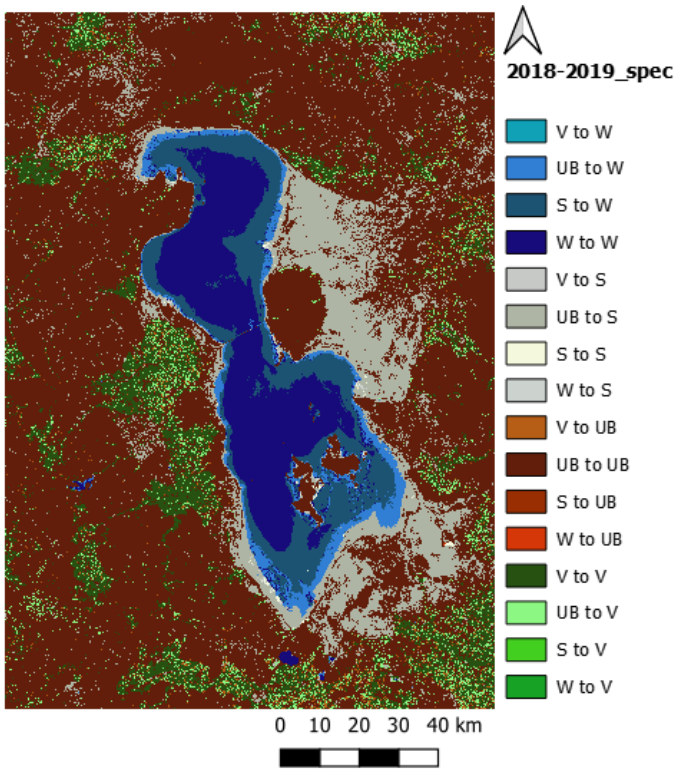

Figure 44:changing map from 2018 to 2019 using spectral angle mapping

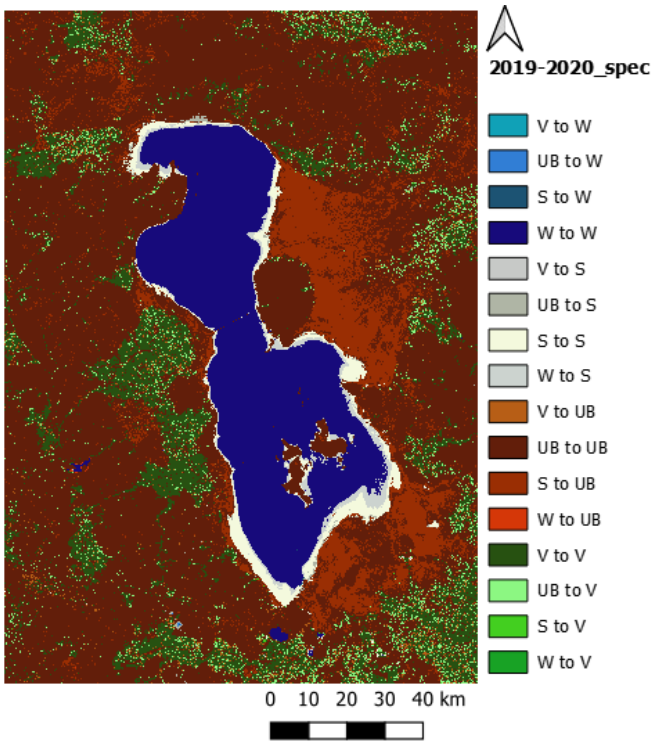

Figure 45:changing map from 2019 to 2020 using spectral angle mapping

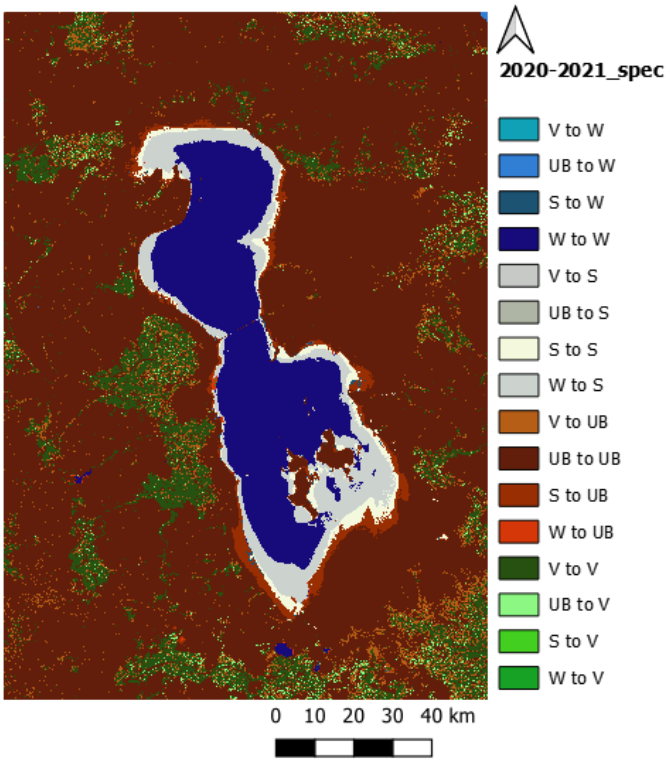

Figure 46:changing map from 2020 to 2021 using spectral angle mapping

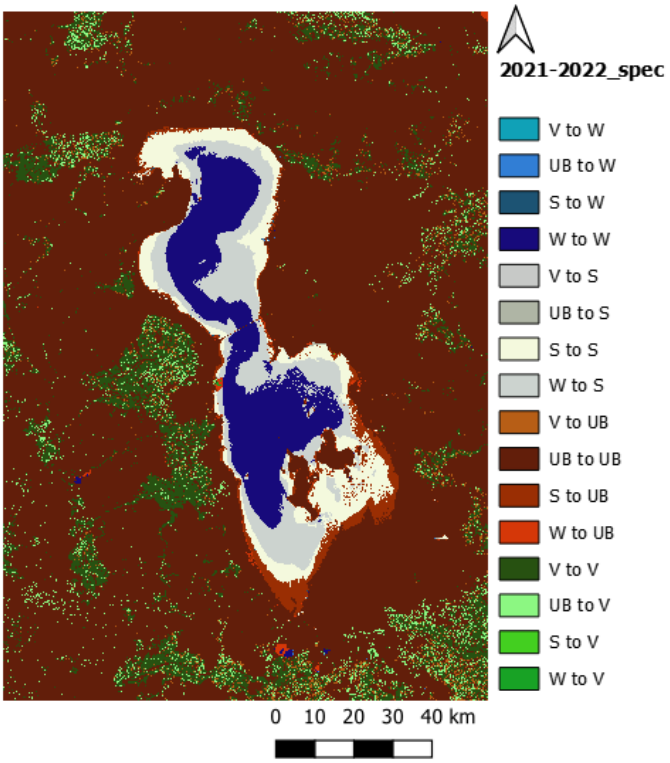

Figure 47:changing map from 2021 to 2022 using spectral angle mapping

The area of different classes and the area of changing map are shown in table 15 to 18. According to table 15 and 16, the area of change of water to salt almost has increased year by year. Based on minimum distance method, these changes were 0.5 Km2 from 2018 to 2019, 167 Km2 from 2019 to 2020, 967 Km2 from 2020 to 2021 and 935 Km2 from 2021 to 2022. According to spectral angle mapping method, these changes were 20 Km2 from 2018 to 2019, 220 Km2 from 2019 to 2020, 847 Km2 from 2020 to 2021 and 986 Km2 from 2021 to 2022.

According to the results of both methods (table 17 and 18) the area of water increased from 2018 to 2019, the area decreased very slightly from 2019 to 2020 and then from 2020 to 2022 decreased year by year. Based on the minimum distance method, the amount of water changes increased by 109% from 2018 to 2019, and decreased by 1% from 2019 to 2020 (water has remained almost constant), decreased by 34% from 2020 to 2021, decreased by 39% from 2021 to 2022. These changes according to the results of spectral angle mapping method are as follows: increased by 92%, decreased by 7%, decreased by 27% and decreased by 45%. The percentage of lake water reduction has increased year by year from 2019 to 2022. Also according to the results of minimum distance and spectral angle mapping methods, the amount of water has decreased by 17% and 27% respectively from 2019 to 2022. Salt has increased by 27% and 45% also Vegetation has increased by about 8% and 10% based on minimum distance method and spectral angle mapping respectively from 2019 to 2022.

Table 15: Area of changing map -minimum distance method

changes	Area from 2018 to 2019(Km²)	Area from 2019 to 2020(Km²)	Area from 2020 to 2021(Km²)	Area from 2021 to 2022(Km²)
Vegetation to Water	1.9458	1.5525	0.5724	0.0441
Urban Area and Bare Soil to Water	520.0614	139.2516	2.3976	7.3008
Salt to Water	1258.4997	0.1962	0.4212	74.2986
Water to Water	1599.3306	3189.1491	2199.3453	1254.0294
Vegetation to Salt	0.4374	1.2654	0.3123	0.0243
Urban Area and Bare Soil to Salt	830.3679	185.1291	9.0099	2.7549
Salt to Salt	16.4862	413.4429	189.1251	690.7023
Water to Salt	0.4311	167.0157	967.338	934.4493
Vegetation to Urban Area and Bare Soil	523.1601	199.9809	1509.8769	250.2522
Urban Area and Bare Soil to Urban Area and Bare Soil	15206.382	13991.6358	14435.3133	16009.7643
Salt to Urban Area and Bare Soil	5.2065	433.0116	575.9001	400.7691
Water to Urban Area and Bare Soil	16.6932	17.4699	161.8857	12.9474
Vegetation to Vegetation	1528.101	1671.4368	1603.3752	1551.4191
Urban Area and Bare Soil to Vegetation	345.6171	1435.4253	195.3774	663.156
Salt to Vegetation	0.0009	1.0719	1.4067	0.0153
Water to Vegetation	0.5166	6.2028	1.5804	1.3104

Table 16:Area of changing map -spectral angle mapping method

changes	Area from 2018 to 2019(Km²)	Area from 2019 to 2020(Km²)	Area from 2020 to 2021(Km²)	Area from 2021 to 2022(Km²)
Vegetation to Water	0.2817	0.0036	0.0072	0.0009
Urban Area and Bare Soil to Water	440.0847	1.1853	3.8871	1.2042
Salt to Water	1187.6265	1.467	22.2021	2.2302
Water to Water	1727.5734	3132.2439	2274.8625	1271.2608
Vegetation to Salt	3.5496	1.0224	0.0036	0.0423
Urban Area and Bare Soil to Salt	2443.4523	49.8906	0.5787	3.825
Salt to Salt	14.7006	398.5434	266.2686	749.637
Water to Salt	19.5057	219.582	847.2015	986.4576
Vegetation to Urban Area and Bare Soil	259.3188	288.4032	919.6587	324.9585
Urban Area and Bare Soil to Urban Area and Bare Soil	13300.4637	12911.8761	15079.6071	15836.2947
Salt to Urban Area and Bare Soil	0.2439	2074.2912	379.8477	362.0997
Water to Urban Area and Bare Soil	1.1898	3.6279	12.4659	42.2118
Vegetation to Vegetation	1794.3552	2165.8176	1851.4314	1721.6451
Urban Area and Bare Soil to Vegetation	660.8547	598.2642	194.1255	550.2555
Salt to Vegetation	0.0063	6.9066	0.72	0.0855
Water to Vegetation	0.0306	0.1125	0.3699	1.0287

Table 17:Area of different parts-minimum distance method

class	Area 2018 (Km²)	Area 2019 Km²)	Area 2020 (Km²)	Area 2021 (Km²)	Area 2022 (Km²)
Water	1616.9715	3379.8375	3330.1494	2202.7365	1335.6729
Salt	1280.1933	847.7226	766.8531	1165.7853	1627.9308
Urban Area and Bare Soil	16902.4284	15751.4418	14642.0982	16682.976	16673.733
Vegetation	2053.6443	1874.2356	3114.1368	1801.7397	2215.9008

Table 18:Area of different parts-spectral angle mapping method

class	Area 2018 (Km²)	Area 2019 Km²)	Area 2020 (Km²)	Area 2021 (Km²)	Area 2022 (Km²)
Water	1748.2995	3355.5663	3134.8998	2300.9589	1274.6961
Salt	1202.5773	2481.2082	669.0384	1114.0524	1739.9619
Urban Area and Bare Soil	16844.8554	13561.2162	15278.1984	16391.5794	16565.5647
Vegetation	2057.5053	2455.2468	2771.1009	2046.6468	2273.0148

4 conclusion

According to the obtained results of changing map, the area of water changed to salt has increased year by year.

Regarding the trend of changes in the area of the lake, according to the figure 48, the water area of the lake increased from 2018 to 2019 and then decreased year by year. First year from 2018 to 2019, according to the results of minimum distance method, the lake water increased about 109%. after that, from 2019 to 2020, it decreased about 1%. From 2020 to 2021, it decreased 34% and from 2021 to 2022, 39%. These changes according to the results of spectral angle mapping, from the first year to the fourth year, they are 92% increase, 7% decrease, 27% decrease and 45% decrease respectively.

Also, during 5 years from 2018 to 2022, the area of the lake has decreased and according to the results of classification by minimum distance method, the water of the lake has decreased by almost 17% from 2018 to 2022 and by spectral angle mapping by about 27%. Also from 2018 to 2022, Vegetation has increased by minimum distance method and spectral angle mapping approximately 8% and 10% respectively. In fact, as the lake water becomes drier, the amount of salt around it increases, which the figure 48 also shows.

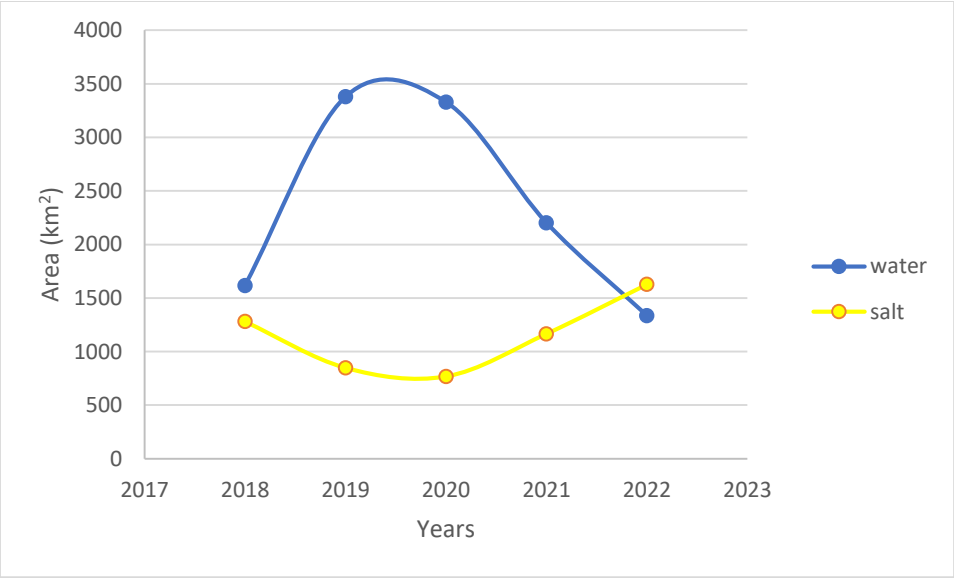

Figure 48: changing the area of water and salt of Urmia Lake – minimum distance

According to the previous researches, since 1995, the lake has experienced catastrophic desiccation, and its trend continues to move decreasing.(Rokni *et al.*, 2014; Schulz *et al.*, 2020), and in this study, confirming previous results, the drying process of the lake can be seen during 2019 to 2022 and especially in 2022, the water area of the lake has decreased drastically.

Based to the results of the classification and their comparison with each other, it seems that there is some error in the recognition of different classes (especially spectral angle mapping method in 2019), and in this research, the ground truth samples to check the accuracy are not prepared, so some check in situ would be useful.

Since this study focused on the surface area of water and salt, for future researches by using remote sensing or in site data collection the water level could be associated to investigate the changes in volume and the effects of water depletion on the surrounded area.

5 Bibliography

Agh, N. *et al.* (2008) 'Effects of salinity on survival, growth, reproductive and life span characteristics of Artemia populations from Urmia Lake and neighboring lagoons.', *Pakistan journal of biological sciences: PJBS*, 11(2), pp. 164–172.

Aurrocoechea, I. and Pethick, J.S. (1986) 'The Coastline-Its Physical and Legal Definition', *Int'l J. Estuarine & Coastal L.*, 1, p. 29.

Ball, G.H. and Hall, D.J. (1965) *ISODATA, a novel method of data analysis and pattern classification*. Stanford research inst Menlo Park CA.

Barnes, B.D. and Wurtsbaugh, W.A. (2015) 'The effects of salinity on plankton and benthic communities in the Great Salt Lake, Utah, USA: a microcosm experiment', *Canadian Journal of Fisheries and Aquatic Sciences*, 72(6), pp. 807–817.

Bioeconomics, I. (2012) 'Economic significance of the Great Salt Lake to the State of Utah', *Great Salt Lake Advisory Council, Utah, Salt Lake City* [Preprint].

Blomqvist, S., Gunnars, A. and Elmgren, R. (2004) 'Why the limiting nutrient differs between temperate coastal seas and freshwater lakes: A matter of salt', *Limnology and oceanography*, 49(6), pp. 2236–2241.

Chaudhari, S. *et al.* (2018) 'Climate and anthropogenic contributions to the desiccation of the second largest saline lake in the twentieth century', *Journal of Hydrology*, 560, pp. 342–353.

Cohen, J. (1960) 'A coefficient of agreement for nominal scales', *Educational and psychological measurement*, 20(1), pp. 37–46.

Congalton, R.G. (2009) 'Accuracy and error analysis of global and local maps: Lessons learned and future considerations', *Remote Sensing of Global Croplands for Food Security*, 441, pp. 47–55.

Congalton, R.G., Oderwald, R.G. and Mead, R.A. (1983) 'Assessing Landsat classification accuracy using discrete multivariate analysis statistical techniques', *Photogrammetric engineering and remote sensing*, 49(12), pp. 1671–1678.

Dariane, A. *et al.* (2019) 'Urmia Lake desiccation and the signs of local climate changes', *Journal of Hydraulic Structures*, 5(2), pp. 1–17.

Du, Z. *et al.* (2012) 'Estimating surface water area changes using time-series Landsat data in the Qingjiang River Basin, China', *Journal of Applied Remote Sensing*, 6(1), pp. 063609–063609.

Duan, Z. and Bastiaanssen, W.G.M. (2013) 'Estimating water volume variations in lakes and reservoirs from four operational satellite altimetry databases and satellite imagery data', *Remote Sensing of Environment*, 134, pp. 403–416. Available at: https://doi.org/10.1016/j.rse.2013.03.010.

Eimanifar, A. and Mohebbi, F. (2007) 'Urmia Lake (northwest Iran): a brief review', *Saline systems*, 3(1), p. 5.

Fagherazzi, S. *et al.* (2019) 'Variations in Persistence and Regenerative Zones in Coastal Forests Triggered by Sea Level Rise and Storms', *Remote Sensing*, 11(17), p. 2019. Available at: https://doi.org/10.3390/rs11172019.

Fath, B. (2018) *Encyclopedia of ecology*. Elsevier.

Fathian, F. *et al.* (2016) 'Trends in hydrological and climatic variables affected by four variations of the Mann-Kendall approach in Urmia Lake basin, Iran', *Hydrological Sciences Journal*, 61(5), pp. 892–904.

Frank, M.G. and Conover, M.R. (2017) 'Weather and prey availability affect the timing of fall migration of Eared Grebes (Podiceps nigricollis) from Great Salt Lake', *The Wilson Journal of Ornithology*, 129(1), pp. 98–111.

Hardie, L.A., Smoot, J.P. and Eugster, H.P. (1978) 'Saline lakes and their deposits: a sedimentological approach', *Modern and ancient lake sediments*, pp. 7–41.

Hereher, M.E. (2015) 'Assessing the dynamics of El-Rayan lakes, Egypt, using remote sensing techniques', *Arabian Journal of Geosciences*, 8, pp. 1931–1938.

Hesami, A. and Amini, A. (2016) 'Changes in irrigated land and agricultural water use in the Lake Urmia basin', *Lake and Reservoir Management*, 32(3), pp. 288–296.

Ho, L.T. and Goethals, P.L. (2019) 'Opportunities and challenges for the sustainability of lakes and reservoirs in relation to the Sustainable Development Goals (SDGs)', *Water*, 11(07), p. 1462.

Hussain, M. *et al.* (2013) 'Change detection from remotely sensed images: From pixel-based to object-based approaches', *ISPRS Journal of photogrammetry and remote sensing*, 80, pp. 91–106.

Karasiak, N. and Perbet, P. (2018) 'Remote Sensing of Distinctive Vegetation in Guiana Amazonian Park', in *QGIS and Applications in Agriculture and Forest*. John Wiley & Sons, Ltd, pp. 215–245. Available at: https://doi.org/10.1002/9781119457107.ch7.

Karbassi, A. *et al.* (2010) 'Environmental impacts of desalination on the ecology of Lake Urmia', *Journal of Great Lakes Research*, 36(3), pp. 419–424.

Khazaei, B. *et al.* (2019) 'Climatic or regionally induced by humans? Tracing hydro-climatic and land-use changes to better understand the Lake Urmia tragedy', *Journal of hydrology*, 569, pp. 203–217.

Knorn, J. *et al.* (2009) 'Land cover mapping of large areas using chain classification of neighboring Landsat satellite images', *Remote Sensing of Environment*, 113(5), pp. 957–964.

Kruse, F.A. *et al.* (1993) 'The spectral image processing system (SIPS)—interactive visualization and analysis of imaging spectrometer data', *Remote sensing of environment*, 44(2–3), pp. 145–163.

Landsat, N. (7) 'Science data users handbook', *Availabe online http//landsathandbook. gsfc. nasa. gov/inst_cal/prog_sect8_2. html (7)(accessed 11 March 2011), 7AD* [Preprint].

Lillesand, T., Kiefer, R.W. and Chipman, J. (2015) *Remote sensing and image interpretation*. John Wiley & Sons.

Liu, Y., Wang, Y. and Zhang, J. (2012) 'New machine learning algorithm: Random forest', in *Information Computing and Applications: Third International Conference, ICICA 2012, Chengde, China, September 14-16, 2012. Proceedings 3*. Springer, pp. 246–252.

Lotfi, A. (2012) 'Lake Uromiyeh: a concise baseline report', *Impel Review Initiative, Department of Environment, United Nations Development Program, New York, New York, USA* [Preprint].

Lyu, H. *et al.* (2018) 'Long-term annual mapping of four cities on different continents by applying a deep information learning method to landsat data', *Remote Sensing*, 10(3), p. 471.

Malahlela, O.E. (2016) 'Inland waterbody mapping: Towards improving discrimination and extraction of inland surface water features', *International Journal of Remote Sensing*, 37(19), pp. 4574–4589.

Mammides, C. (2020) 'A global assessment of the human pressure on the world's lakes', *Global Environmental Change*, 63, p. 102084.

Messager, M.L. *et al.* (2016) *Estimating the volume and age of water stored in global lakes using a geo-statistical approach, Nat. Commun., 7, 13603*.

Micklin, P. (2016) 'The future Aral Sea: hope and despair', *Environmental Earth Sciences*, 75, pp. 1–15.

Miller, J.R. (1987) 'The Political Economy of Western Water Finance: Cost Allocation and the Bonneville Unit of the Central Utah Project', *American Journal of Agricultural Economics*, 69(2), pp. 303–310.

Nourani, V., DANANDEH MEHR, A. and Azad, N. (2018) 'Trend analysis of hydroclimatological variables in Urmia lake basin using hybrid wavelet Mann–Kendall and Şen tests', *Environmental Earth Sciences*, 77. Available at: https://doi.org/10.1007/s12665-018-7390-x.

Null, S.E. and Wurtsbaugh, W.A. (2020) 'Water development, consumptive water uses, and Great Salt Lake', *Great Salt Lake biology: A terminal Lake in a time of change*, pp. 1–21.

Onyango, D.O. and Opiyo, S.B. (2022) 'Detection of historical landscape changes in Lake Victoria Basin, Kenya, using remote sensing multi-spectral indices', *Watershed Ecology and the Environment*, 4, pp. 1–11. Available at: https://doi.org/10.1016/j.wsee.2021.12.001.

Polykretis, C., Grillakis, M.G. and Alexakis, D.D. (2020) 'Exploring the impact of various spectral indices on land cover change detection using change vector analysis: A case study of Crete Island, Greece', *Remote Sensing*, 12(2), p. 319.

Potić, I. and Potić, M. (2017) 'REMOTE SENSING MACHINE LEARNING ALGORITHMS IN ENVIRONMENTAL STRESS DETECTION - CASE STUDY OF PAN-EUROPEAN SOUTH SECTION OF CORRIDOR 10 IN SERBIA', *Bulletin of Natural Sciences Research*, 7(2). Available at: https://doi.org/10.5937/univtho7-14957.

Read, J.M. and Torrado, M. (2009) 'Remote Sensing', in R. Kitchin and N. Thrift (eds) *International Encyclopedia of Human Geography*. Oxford: Elsevier, pp. 335–346. Available at: https://doi.org/10.1016/B978-008044910-4.00508-3.

Richards, J.A. and Jia, X. (2006) 'Interpretation of hyperspectral image data', *Remote Sensing Digital Image Analysis: An Introduction*, pp. 359–388.

Roberts, A.J. (2013) 'Avian diets in a saline ecosystem: Great Salt Lake, Utah, USA', *Human-Wildlife Interactions*, 7(1), pp. 158–168.

Rokni, K. *et al.* (2014) 'Water feature extraction and change detection using multitemporal Landsat imagery', *Remote sensing*, 6(5), pp. 4173–4189.

Ryan, E. (2015) 'The public trust doctrine, private water allocation, and mono lake: the historic saga of national audubon society v. Superior Court', *Envtl. L.*, 45, p. 561.

Sattari, M.T. *et al.* (2020) 'Trend and abrupt change analysis in water quality of Urmia Lake in comparison with changes in lake water level', *Environmental monitoring and assessment*, 192, pp. 1–16.

Schmidt, M., Gonda, R. and Transiskus, S. (2021) 'Environmental degradation at Lake Urmia (Iran): exploring the causes and their impacts on rural livelihoods', *GeoJournal*, 86, pp. 2149–2163.

Schulz, S. *et al.* (2020) 'Climate change or irrigated agriculture–what drives the water level decline of Lake Urmia', *Scientific reports*, 10(1), pp. 1–10.

Sim, J. and Wright, C.C. (2005) 'The kappa statistic in reliability studies: use, interpretation, and sample size requirements', *Physical therapy*, 85(3), pp. 257–268.

Singh, A. (1989) 'Review article digital change detection techniques using remotely-sensed data', *International journal of remote sensing*, 10(6), pp. 989–1003.

Stehman, S. (1996) 'Estimating the kappa coefficient and its variance under stratified random sampling', *Photogrammetric Engineering and Remote Sensing*, 62(4), pp. 401–407.

Sun, F. *et al.* (2012) 'Comparison and improvement of methods for identifying waterbodies in remotely sensed imagery', *International journal of remote sensing*, 33(21), pp. 6854–6875.

Tang, J. *et al.* (2019) 'Spatial–temporal landscape pattern change under rapid urbanization', *Journal of Applied Remote Sensing*, 13(2), pp. 024503–024503.

Vaheddoost, B. *et al.* (2015) 'Decision tree for measuring the interaction of hyper-saline lake and coastal aquifer in Lake Urmia', in *Watershed Management 2015*, pp. 62–71.

Vaheddoost, B. and Aksoy, H. (2017) 'Structural characteristics of annual precipitation in Lake Urmia basin', *Theoretical and Applied Climatology*, 128, pp. 919–932.

Verpoorter, C., Kutser, T. and Tranvik, L. (2012) 'Automated mapping of water bodies using Landsat multispectral data', *Limnology and Oceanography: Methods*, 10(12), pp. 1037–1050.

Waiser, M.J. and Robarts, R.D. (2009) 'Saline inland waters'.

White, J.S., Null, S.E. and Tarboton, D.G. (2015) 'How do changes to the railroad causeway in Utah's Great Salt Lake affect water and salt flow?', *PloS one*, 10(12), p. e0144111.

Williams, W.D. (2002) 'Environmental threats to salt lakes and the likely status of inland saline ecosystems in 2025', *Environmental conservation*, 29(2), pp. 154–167.

Woolway, R.I. *et al.* (2020) 'Global lake responses to climate change', *Nature Reviews Earth & Environment*, 1(8), pp. 388–403.

Wurtsbaugh, W.A. *et al.* (2017) 'Decline of the world's saline lakes', *Nature Geoscience*, 10(11), pp. 816–821.

Yu, Z. *et al.* (2018) 'Land use and land cover classification for Bangladesh 2005 on google earth engine', in *2018 7th International Conference on Agro-geoinformatics (Agro-geoinformatics)*. IEEE, pp. 1–5.

Yu, Z. *et al.* (2019) 'Selection of landsat 8 OLI band combinations for land use and land cover classification', in *2019 8th International Conference on Agro-Geoinformatics (Agro-Geoinformatics)*. IEEE, pp. 1–5.

Zhang, Z. and Moore, J.C. (2014) *Mathematical and physical fundamentals of climate change*. Elsevier.

A Appendix A

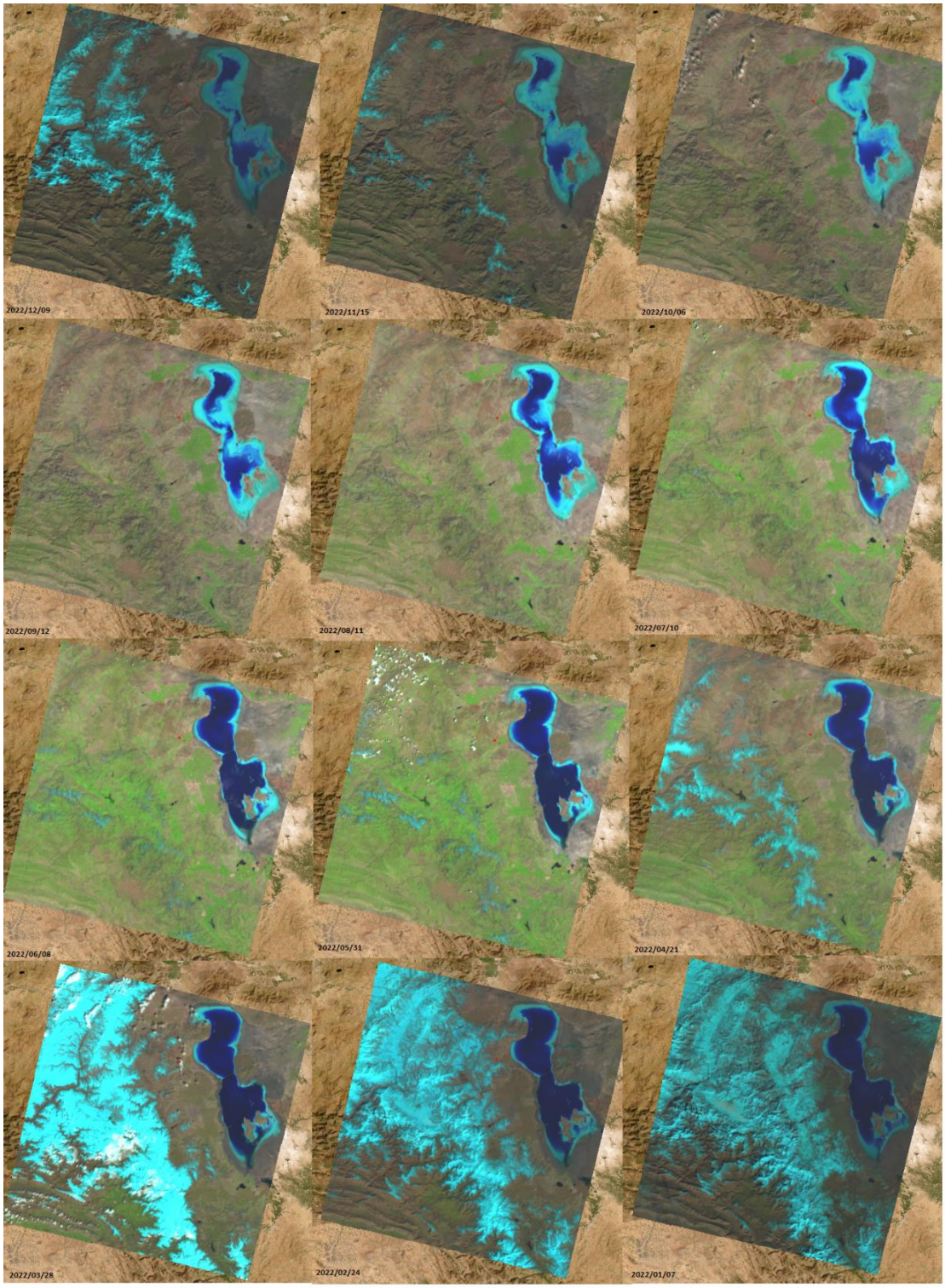

Figure 49:Visual assessment of changes in water surface of Urmia lake in different months of 2022

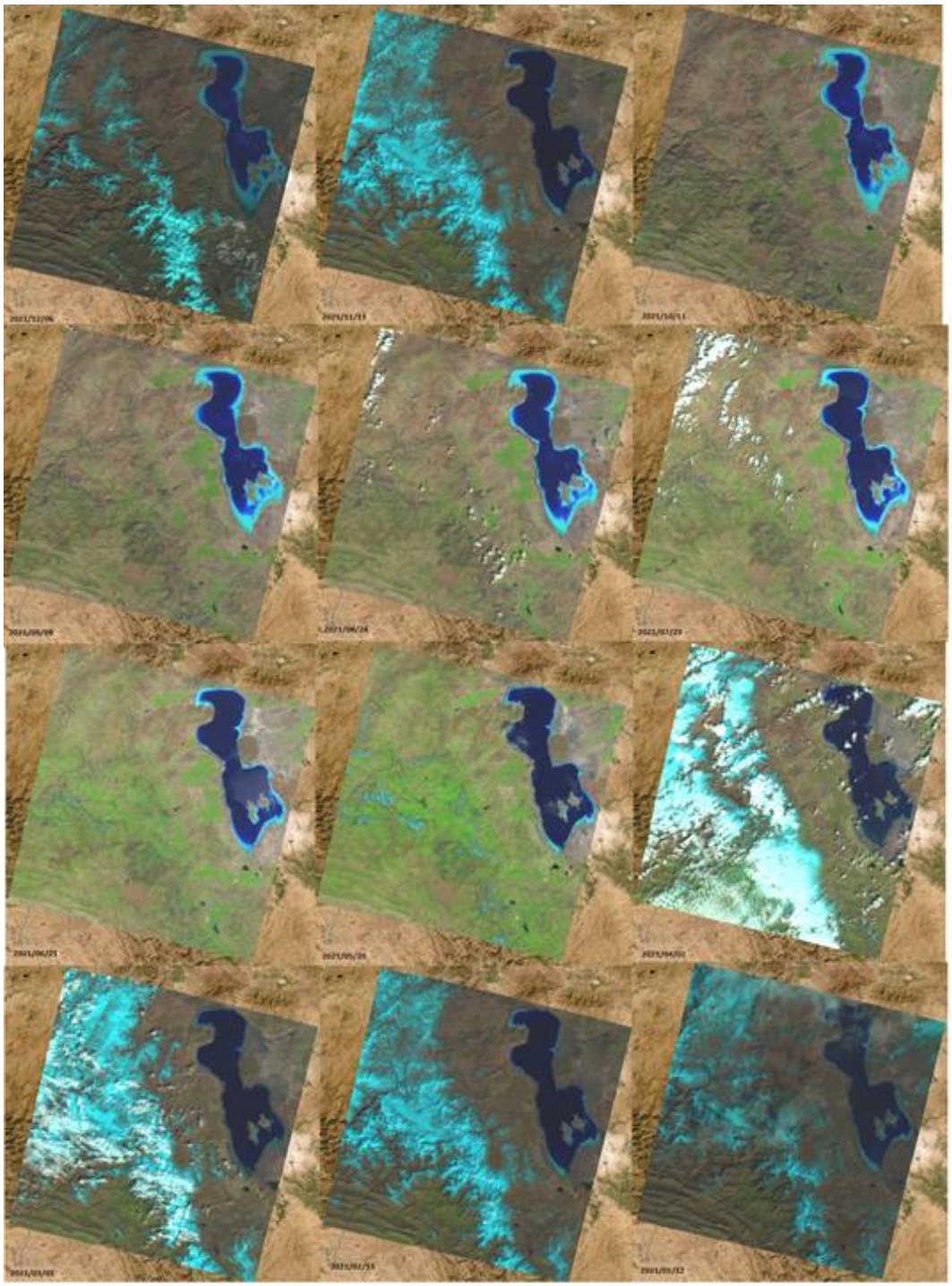

Figure 50:Visual assessment of changes in water surface of Urmia lake in different months of 2021

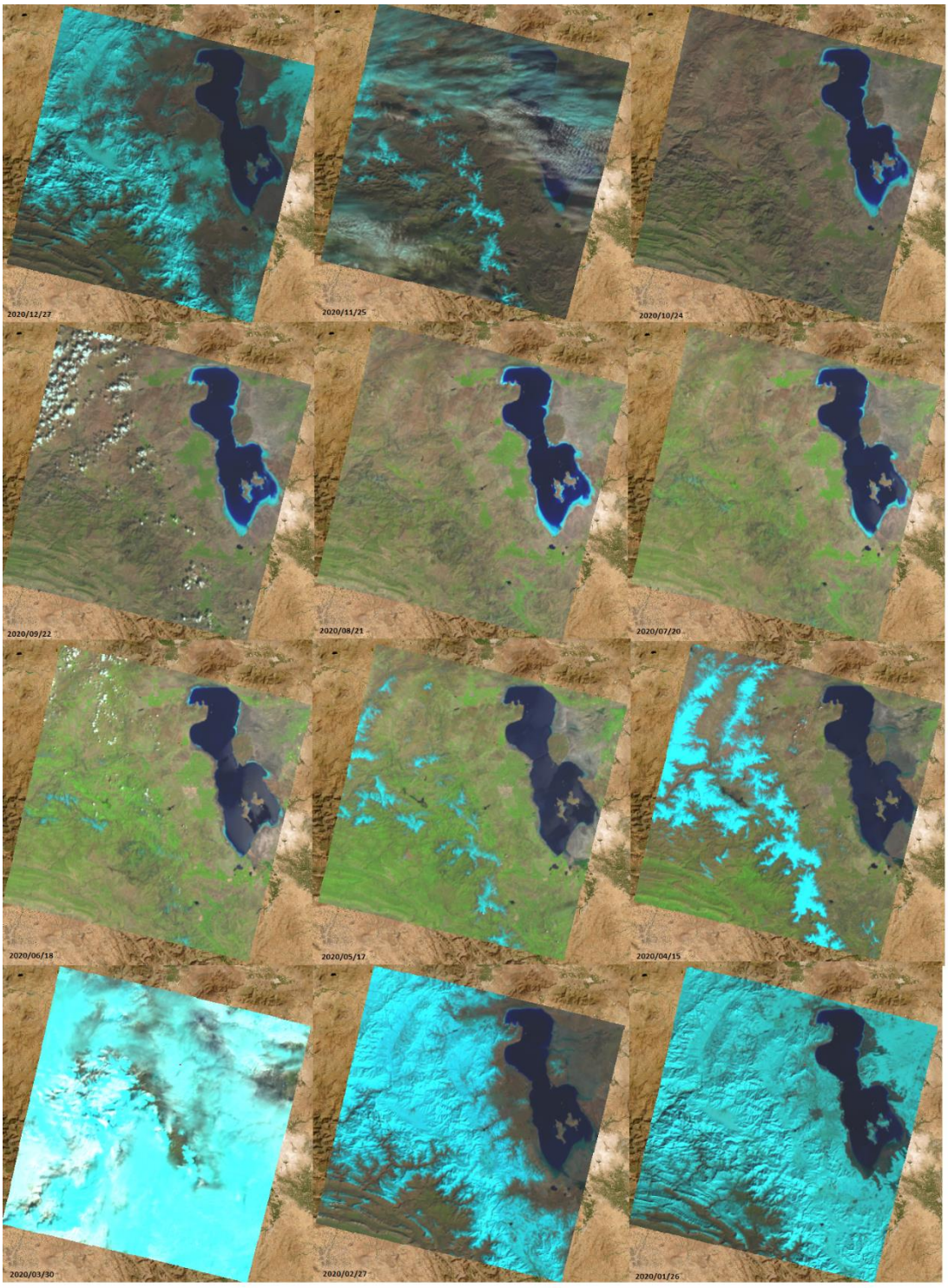

Figure 51:Visual assessment of changes in water surface of Urmia lake in different months of 2020

List of Figures

List of Tables

Acknowledgments

First, I would like to thank my supervisors, Professor Giovanna Sona and Professor Giovanna Venuti, who were always available whenever I had doubts or questions even outside the working hours. I thank them for fully understanding my situation as a new mother and patiently answering my questions to solve my problems.

To conclude, thanks to my husband who is always with me in all the stages and during the master's courses and doing the thesis, he gave me every help he could and encouraged me to finish this master degree.